MULTIPLE NEGATIVE CARBON-ISOTOPE EXCURSIONS DURING THE CARNIAN PLUVIAL EPISODE (LATE TRIASSIC)

Jacopo Dal Corso[1,2,3,4*], Piero Gianolla[2], Manuel Rigo[3,5], Marco Franceschi[3], Guido Roghi[5], Paolo Mietto[3], Stefano Manfrin[3], Béla Raucsik[6], Tamás Budai[7], Hugh C. Jenkyns[8], Claire E. Reymond[4], Marcello Caggiati[2], Giovanni Gattolin[9], Anna Breda[3], Agostino Merico[4,10], Nereo Preto[3]

[1]School of Earth and Environment, University of Leeds, Leeds LS2 9JT, United Kingdom

[2]Department of Physics and Earth Sciences, University of Ferrara, via Saragat 1, 44100 Ferrara, Italy

[3]Department of Earth Sciences, University of Padova, via Gradenigo 6, 35131 Padova, Italy

[4]Leibniz Centre for Tropical Marine Research (ZMT), Fahrenheitstraße 6, 28359 Bremen, Germany

[5]Institute of Geosciences and Earth Resource (IGG - CNR), via Gradenigo 6, 35131 Padova, Italy

[6]Department of Mineralogy, Geochemistry and Petrology, University of Szeged, Egyetem utca 2H-6722, Szeged, Hungary

[7]Geological and Geophysical Institute of Hungary, Stefánia út 14. H-1143, Budapest, Hungary

[8]Department of Earth Sciences, University of Oxford, South Parks Road, Oxford OX1 3AN, UK

[9]Upstream and Technical Services, Eni S.p.A., Via Emilia, 1, 20097 San Donato Milanese, Italy

[10]Faculty of Physics & Earth Sciences, Jacobs University Bremen, 28759 Bremen, Germany

*Corresponding author: J.DalCorso@leeds.ac.uk

KEYWORDS

Carnian Pluvial Episode; Late Triassic; carbon-isotopes; climate change; extinction.

ABBREVIATIONS

CPE = Carnian Pluvial Episode

NCIE = Negative Carbon-Isotope Excursion

LIP = Large Igneous Province

ABSTRACT

The Carnian Pluvial Episode was a phase of global climatic change and biotic turnover that occurred during the early Late Triassic. In marine sedimentary basins, the arrival of huge amounts of siliciclastic sediments, the establishment of anoxic conditions, and a sudden change of the carbonate factory on platforms marked the Carnian Pluvial Episode. The sedimentary changes are closely associated with abrupt biological turnover among marine and terrestrial groups as, for example, an extinction among ammonoids and conodonts in the ocean, and a turnover of the vertebrate fauna and the flora on land. Multiple negative carbon-isotope excursions were recorded during the Carnian Pluvial Episode in both organic matter and marine carbonates suggesting repeated injection of ^{13}C-depleted CO_2 into the ocean–atmosphere system, but their temporal and causal links with the sedimentological and palaeontological changes are poorly understood. We here review the existing carbon-isotope records and present new data on the carbon-isotope composition of organic carbon in selected sections of the western Tethys realm that record the entire Carnian Pluvial Episode. New ammonoid, conodont and sporomorph biostratigraphic data were collected and coupled to an extensive review of the existing biostratigraphy to constrain the age of the sampled sections. The results provide biostratigraphically constrained composite organic carbon-isotope curves for the Carnian, and shed light on the temporal and causal links between the features of the carbon-isotope record that characterize the Carnian Pluvial Episode and the distinct climatic and environmental changes, and biological extinctions and turnovers, that mark this interval. The carbon-isotope records suggest that a series of carbon-cycle perturbations, possibly recording multiple phases of volcanic activity during the emplacement of the Wrangellia Large Igneous Province, disrupted Carnian environments and ecosystems repeatedly over a remarkably long time interval of about 1 million years.

1. INTRODUCTION

During the Carnian age (early Late Triassic), a global climate change took place (Simms and Ruffell, 1989; Preto *et al.*, 2010) later termed the Carnian Pluvial Episode (CPE; Simms and Ruffell, 1989) and dated through biostratigraphic calibration from the Julian 2 to the Tuvalian 2 intervals (*sensu* Mietto *et al.*, 2012; Fig. 1). The CPE was characterized by major environmental changes in continental to shallow- and deeper water settings, and biological turnovers on land and in the ocean (e.g., Schlager and Schöllnberg, 1974; Benton, 1983; Simms and Ruffell 1989; Benton 1991; Krystyn 1991; Simms *et al.*, 1995; Gianolla *et al.*, 1998; Roghi *et al.*, 2004; Hornung and Brandner, 2005; Furin *et al.*, 2006; Keim *et al.*, 2006; Hornung et al., 2007; Rigo *et al.*, 2007; Breda *et al.*, 2009; Preto *et al.*, 2010; Balini *et al.*, 2010; Roghi *et al.*, 2010; Stefani *et al.*, 2010; Arche and López-Gómez, 2013; Martínez-Pérez *et al.*, 2014; Lukeneder and Lukeneder, 2014; Franz *et al.*, 2014; Chen *et al.*, 2015; Dal Corso *et al.*, 2015, 2018; Gattolin *et al.*, 2015; Ruffell *et al.*, 2016; Mueller *et al.*, 2016a,b; Sun *et al.*, 2016; Miller *et al.*, 2017; Dunhill *et al.*, 2017; Bernardi *et al.*, 2018). The onset of the CPE coincided with a perturbation of the carbon cycle characterized by a sharp 2–4‰ negative carbon-isotope excursion (NCIE). The NCIE is found in terrestrial and marine organic matter (biomarkers and total organic carbon) and marine carbonates in stratigraphic sections in Europe and China (Dal Corso *et al.*, 2012, 2015; Muttoni *et al.*, 2014; Mueller *et al.*, 2016a, 2016b; Sun *et al.*, 2016; Miller *et al.*, 2017). This NCIE suggests an injection of large quantities of ^{13}C-depleted CO_2 into the ocean–atmosphere system that is thought to have induced the climate change and be possibly linked to the eruption of the Wrangellia, also called Nikolai, Large Igneous Province (LIP; Dal Corso *et al.*, 2012, 2015; Mueller *et al.*, 2016a; Sun *et al.*, 2016). The emission of large amounts of greenhouse gases into the atmosphere is credited with inducing a global temperature increase estimated as 4–7°C by the examination of the oxygen-isotope signature of conodont apatite from marine successions of the Tethyan realm (Hornung *et al.*, 2007; Rigo and Joachimski 2010; Trotter *et al.*, 2015; Sun *et al.*, 2016). Warming in turn presumably triggered a strong intensification of the hydrological cycle and enhanced continental runoff (e.g. Dal Corso *et al.*, 2015; Sun *et al.*, 2016). The CPE was also coincident with biological turnovers on land and in the ocean (e.g. Simms and Ruffell, 1989; Ruffell *et al.*, 2016).

Palynological records show a widespread turnover of the terrestrial flora from xerophytic to hygrophitic at different palaeolatitudes, and decrease in diversity (Roghi *et al.*, 2010; Kürschner and Herngreen, 2010; Mueller et al., 2016a,b). Many lineages of terrestrial tetrapod became extinct or significantly declined during the CPE with, however, a significant rise in the dinosaurs (Benton, 1983; Benton 1991; Bernardi *et al.*, 2018). The CPE was also associated with a major turnover in marine taxa (Simms and Ruffell 1989; Benton 1991; Simms *et al.*, 1995). Two major events occurred at the Julian–Tuvalian boundary, as illustrated by a prominent extinction of conodonts (Rigo *et al.*, 2007; Martínez-Pérez *et al.*, 2014; Chen *et al.*, 2015) and the crisis of the *Trachyceratinae* ammonoids, the most significant turnover of this group in the entire Triassic Period (Krystyn 1991; Balini *et al.*, 2010).

Despite the common features that mark the CPE worldwide, however, this phase of Earth history appears not to be uniform. The existence of multiple (at least three) prominent humid pulses within the CPE has been shown by stratigraphic and palynostratigraphic investigations in the Southern Alps and Northern Calcareous Alps that were part of the western Tethys domain in the Carnian (Roghi *et al.*, 2010). Distinct large-scale intercalations of coarse siliciclastics that interrupt shallow-water carbonate successions in the north western Tethys, as well as repeated shifts in the composition of the microflora, from xerophytic to hygrophytic forms, are recorded in sedimentary successions (Roghi *et al.*, 2010; Mueller *et al.*, 2016a and references therein). This evidence, coupled with recent age models based on cyclostratigraphy of gamma-ray and elemental abundances (Zhang *et al.*, 2015; Miller *et al.*, 2017), which assign to the CPE a duration of approximately 1.2 Myr, show that this event was not characterized by uniform climatic conditions and a more complex series of events occurred over such an extended period of time. Furthermore, Sun *et al.* (2016) reported three NCIE in bulk carbonates of the Carnian sedimentary succession of South China (Guizhou): at the base of the Julian 2, at the Julian–Tuvalian boundary, and in the Tuvalian 1. Such shifts are not recorded by organic matter from the same stratigraphic succession, which in turn record a long-term negative shift that starts at the base of the Julian 2 and rebounds to pre-excursion values at the top of the Tuvalian 1. However, Miller *et al.* (2017) detected five NCIE in leaf-wax *n*-alkanes and bulk organic matter from the WP borehole 1 drilled in the Carnian

continental succession of Devon (UK). These findings strongly suggest that multiple carbon-cycle perturbations occurred during the CPE.

We here review the evidence of multiple carbon-isotope excursions during the CPE and suggest a connection between its sedimentological record from the Western Tethys and the features of the carbon-isotope curve. We have integrated the existing isotopic records with a high-resolution carbon-isotope stratigraphy, whose age is constrained by ammonoid, conodont and sporomorph biostratigraphy. To this end, we collected new data on the carbon-isotope composition of total organic carbon ($\delta^{13}C_{TOC}$) and wood ($\delta^{13}C_{WOOD}$) in selected sections of the Western Tethys that encompass the stratigraphic range of the entire CPE. We also collected new ammonoid, conodont and sporomorph biostratigraphic data and extensively reviewed the existing biostratigraphic coverage to constrain the age of the sampled sections. The results provide a biostratigraphically very well-constrained organic carbon-isotope reference curve for the Carnian interval, and elucidate the temporal relationships between the geochemical and the climatic, environmental, and biological changes that punctuated the CPE.

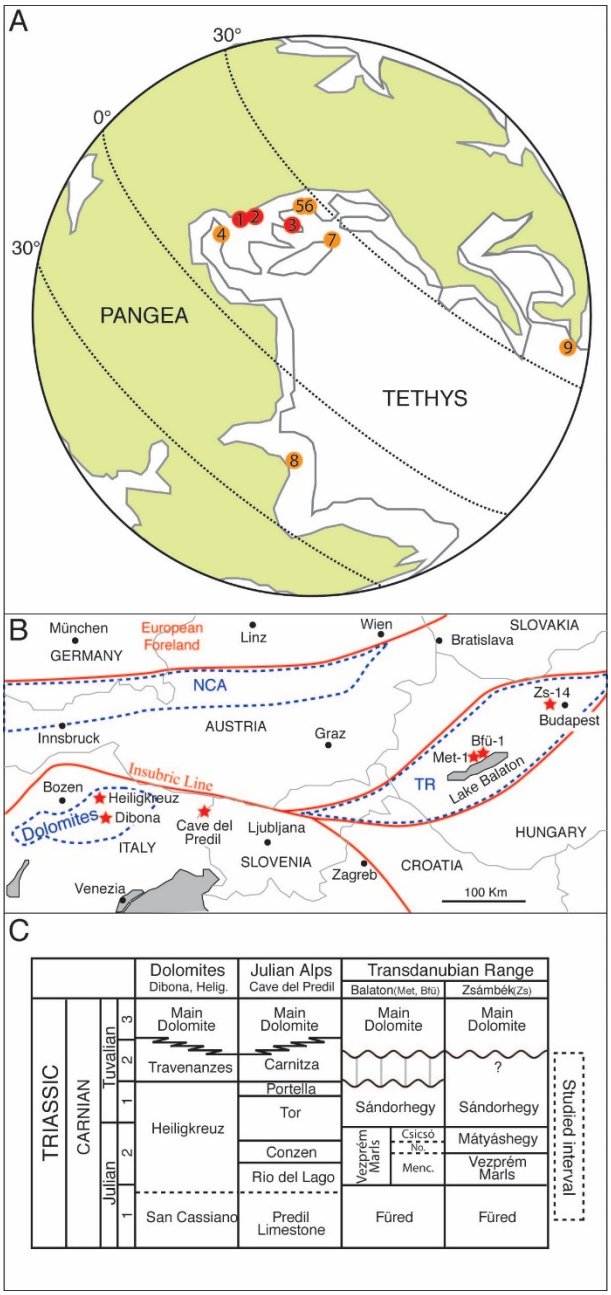

Figure 1. A) Late Triassic palaeogeography (redrawn from Stampfli and Borel, 2002). The red dots show the location of the stratigraphic sections and cores analysed for total organic-carbon isotopes in this study: 1) Dolomites, Italy; 2) Julian Alps, Italy; and 3) Transdanubian Range, Hungary. The orange dots show the location of additional selected successions where sudden siliciclastic inputs and/or major changes in the carbonate factories on platforms are recorded and are stratigraphically well constrained: 4) Lagonegro, Italy; 5) Drau Range, Austria; 6) Lunz, Austria; 7) Turkey; 8) Spiti, India; 9) South China Block, China. B) Map of the study area, including the major tectonic lineaments. The red stars indicate the location of the studied sections. NCA = Northern Calcareous Alps; TR = Transdanubian Range. C) Lithostratigraphic scheme for the Carnian formations in the studied areas. Biostratigraphic constraints from this study and the literature are shown in Fig. 2.

2. GEOLOGICAL SETTING

The studied sedimentary successions are located in the Dolomites-UNESCO World Heritage area (Italy; https://www.dolomitiunesco.it/en/), in the Julian Alps (Italy), and in the Balaton Highland and Zsámbék Basins (Hungary), and belong to the Tethyan realm (Fig. 1A and B).

The Carnian (Julian–Tuvalian) succession of the Dolomites (Fig. 1C and Fig. 2) begins with the marls and calcareous turbidites of the San Cassiano Formation (Julian). The relative modal composition of packstones and grainstones in the San Cassiano Formation, which reflects the composition of the carbonate producers on the coeval platforms (Cassian Dolomite), show high contents of microbial elements such as oncoids, calcimicrobes, and intraclasts with clotted peloidal fabric (Preto, 2012). Such microbial-dominated composition abruptly changes in the uppermost part of the San Cassiano Formation (lowermost Heiligkreuz Formation), in correspondence with the negative carbon-isotope excursion that marks the onset of the CPE. Ooids and skeletal grains become the most abundant components, and the microbial carbonates reduce to less than 10% of rock volume (Gattolin *et al.*, 2015). This change in facies is interpreted as evidence for the crisis of the highly productive early Carnian microbially dominated platforms, which were replaced by less productive metazoan ramps (Gattolin *et al.*, 2015; Dal Corso *et al.*, 2015). Above the San Cassiano Formation, the coarse silicislastics, clays, and marls mixed with skeletal and oolitic carbonates of the Heiligkeuz Formation were deposited (Neri *et al.*, 2007; Breda *et al.*, 2009; Stefani *et al.*, 2010). The Heiligkreuz Formation is locally more than 100 m thick and represents the rapid infilling of the early Carnian basins as a consequence of the increasing continental runoff during the CPE. It is followed stratigraphically by the clays and dolomites of the Travenanzes Formation (Tuvalian), which was deposited in a marginal marine dryland coastal system (Breda and Preto, 2011). The investigated stratigraphic sections in the Dolomites, which encompass the Heiligkreuz–Travenanzes Formations, are biostratigraphically very well constrained by ammonoids, conodonts, and sporomorphs (Fig. 2; e.g., Breda et al., 2009; Maron *et al.*, 2017).

The locality studied in the Julian Alps is the classical Cave del Predil area (formerly “Raibl”) (Fig. 1C). Here, the Carnian succession starts with the black laminated limestone of the Predil Limestone (Julian). The age of this unit has been re-assigned to the *aonoides* ammonoid zone

(see results). Above, a thick (>1000 m) succession of silt and marl alternates with lime mudstone to packstone, locally dolomitized, with abundant skeletal grains (Rio del Lago, Conzen, Tor Formations and Portella Dolomite, upper Julian to lower Tuvalian; De Zanche *et al.*, 2000). The remaining portion of the Tuvalian is represented by mainly nodular, cherty lime mudstone of the Carnitza Formation, which lies conformably on top of the Portella Dolomite (Fig. 1C; Gianolla *et al.*, 2003; Caggiati *et al.*, 2007). The age of the Cave del Predil section is constrained by ammonoids, conodonts, and sporomorphs (Fig. 2; this study, section 4.1; De Zanche *et al.*, 2000; Gianolla *et al.*, 2003; Roghi *et al.*, 2004).

In the Balaton Highland of the Transdanubian Range, a relatively thick marl-dominated succession suggests an increased input of clay and silt from distal sources and lime mud from the neighbouring shallow-water areas during the Julian (Veszprém Marl, Fig. 2; Budai and Haas, 1997; Haas and Budai, 1999). Above, shales with variable carbonate content (Sándorhegy Formation) record the infill of the intra-platform basins during the Late Carnian (Tuvalian) and apparently levelled the topography, on which the peritidal Main Dolomite was deposited. The stratigraphic successions of the Transdanubian Range are biostratigraphically well constrained with ammonoids, sporomorphs, and conodonts (Fig. 2; Budai *et al.*, 1999). Similarly, the succession in the Zsámbék Basin of the Transdanubian Range (Fig. 1C and 2) starts with the Budaörs Dolomite, which represents a carbonate platform inherited from the Ladinian, while coeval carbonate platforms (Ederics Limestone) and intra-platform basins (Füred Limestone) existed in the Balaton Highland and in the Bakony Hills. The Budaörs Dolomite is overlain by grey laminated marls with thin limestone intercalations, which represent increasing siliciclastic content (Veszprém Marl; Early Julian). Up-section, the Veszprém Marl is overlain by a thin-bedded cherty limestone and dolomite (Mátyáshegy Formation, Fig. 1C; Haas and Budai, 2004) with a depauperate foraminifer, ostracod and conodont fauna suggesting a restricted basinal environment (Kristan-Tollmann *et al.*, 1991; Góczán and Oravecz–Scheffer, 1996a,b). This part of the succession is followed by layers of dark grey dolomitic calcareous marl with foraminifera- and ostracod-bearing mudstone and wackestone (Sándorhegy Formation; Haas and Budai, 2004).

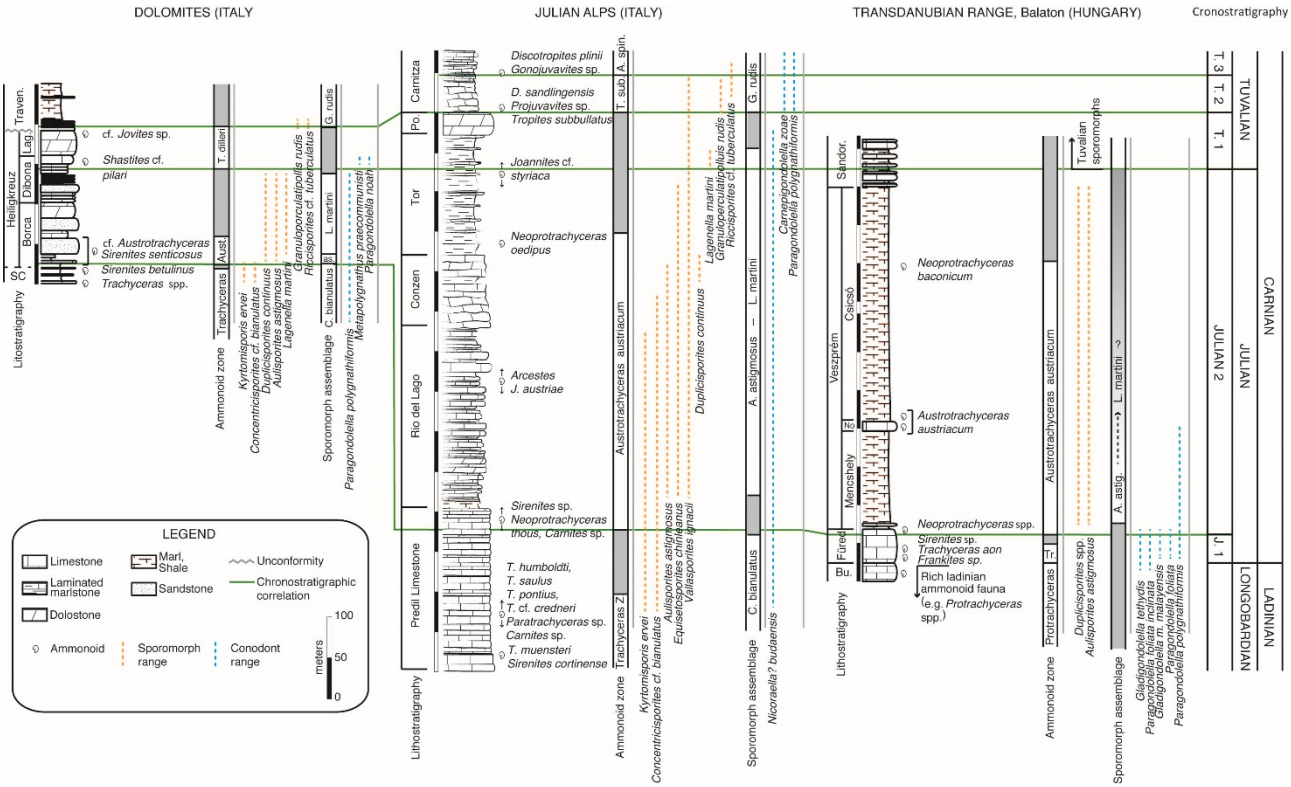

Figure 2. Biostratigraphic constraints (ammonoids, sporomorphs, and conodonts) of the studied Carnian successions in the Dolomites (Italy), Julian Alps (Italy), and Transdanubian Range (Hungary). Data from the Dolomites are summarized from Breda *et al.* (2009), Dal Corso *et al.* (2012), and Maron *et al.* (2017). Julian Alps: Ammonoid, sporomorph, and conodont data of the Julian Alps are from this study, De Zanche *et al.* (2000), Lieberman (1978), Gianolla *et al.* (2003), Roghi (2004), and Roghi *et al.* (2010). Ammonoid, sporomorph, and conodont data of the Transdanubian Range are from Dosztály *et al.* (1989), Kovács *et al.* (1991), Góczán *et al.* (1991), Góczán and Oravecz-Scheffer (1996), Vörös (1998), Budai *et al.* (1999), and Dal Corso *et al.* (2015). Dark grey areas in the biostratigraphic zonations represent intervals of uncertain biostratigraphic attribution. Abbreviations: Tuv. = Tuvalian; J. 1. = Julian 1; T. 1 = Tuvalian 1; SC = San Cassiano Formation; Lag. = Lagazuoi Member; Traven. = Travenanzes Formation; Po. = Portella Limestone; Sandor = Sandorhégy Formation; No = Nosztor Limestone; Aust. = *austriacum*; Tr. = *Trachyceras*; Tropit. = *Tropites*; A. as. = *A. astigmosus*; L. mar = *L. martini*. The figure is modified after Roghi *et al.* (2010) and Dal Corso *et al.* (2015).

3. METHODS

3.1 Sections

Sections from the Dolomites and Julian Alps, and cores from the Transdanubian Range, have been sampled to strengthen the biostratigraphy and produce new organic carbon-isotope data. In the Dolomites, the Milieres-Dibona and Heiligkreuz sections encompass the Borca, Dibona and Lagazuoi Members of the Heiligkreuz Fm. (Fig. 2). The Miliers-Dibona sections have been measured and described by Preto and Hinnov (2003), Breda *et al.* (2009), Dal Corso *et al.* (2012), Maron *et al.* (2017). The overlying Travenanzes Fm. has been sampled in the Dibona section. In both the Heiligkreuz and Milieres-Dibona sections the lower part of Borca Member (lowermost Heiligkreuz Fm.), i.e., the portion between the Milieres and the Dibona segments, is missing, as in the rest of the Dolomites, because of the unstable nature of these clayey deposits (e.g., Neri *et al.*, 2001). The Miliers-Dibona and Heiligkreuz sections can be physically correlated bed by bed, being part of the same sedimentary succession. In the Julian Alps, the Rio Conzen, Rio delle Cascate, and Portella sections of the Cave del Predil area have been also sampled. These sections were previously studied and described by De Zanche *et al.* (2000) and Roghi (2004). The Rio Conzen and Rio delle Cascate sections are adjacent and can be easily correlated to each other using marker beds. They encompass the Predil Limestone, Rio del Lago Fm., the Conzen Fm., and part of the Tor Fm. The Portella section encompasses the upper Tor Formation, the Portella Limestone and the Carnitza Fm. A part of the Tor Fm., from the top of the Rio Conzen-Rio delle Cascate section to the base of the Portella section, could not be sampled due to the nature of the outcrops. In the Transdanubian Range, cores from the Balaton area and the Zsámbék basins have been sampled. These cores have been previously described and studied for clay mineralogy by Rostási *et al.* (2011). The Met-1 core encompasses the Mencshely, Nosztor Limestone and Csicsó members of the Vesprém Marls of the Balaton area. The Zs-14 core encompasses the uppermost Veszprem Marls, the Mátyáshegy Fm., and the Sándorhegy Fm. of the Zsámbék Basin.

3.2 New biostratigraphic constraints

Three hundred and forty-eight (348) unpublished ammonoid determinations from Cave del Predil (formerly the "Raibl" area), from museum collections and own new findings, were used to constrain the age of lithostratigraphic units of the Julian Alps. The new material studied for this work was collected from the Predil Limestone on the left side of the Fella Valley near Cave del Predil (formerly "Raibl"), Tarvisio (Julian Alps). Ammonoid specimens are stored at the: Geologische Bundesanstalt, Vienna, Austria; Museo Friulano di Storia Naturale, Udine, Italy; Museo Paleontologico Cittadino, Monfalcone, Italy; and Museo Geologico Universitario, Padova, Italy. A complete list of these ammonoids with additional information is given in Table 1S (supplementary materials). Only a few specimens were collected in the lower Rio Del Lago Formation. Most of the material occurs as highly compressed specimens, and only rarely are the ventral parts visible. This state of preservation makes the determination at the species level difficult and sometimes impossible.

Investigated conodonts were collected in rocks from sections in the Julian Alps, and from the matrix of ammonoid samples. Conodonts were extracted by dissolving 1-8 kg samples of carbonate rock in diluted formic acid at room temperature until the reaction was completed. The residuals were then gently washed and sieved. Conodont elements were picked manually from the fraction > 100 μm.

Sporomorphs were extracted from samples at the base of the Rio del Lago Formation also using standard techniques (e.g. Roghi *et al.*, 2004). Samples were powdered and treated with HCl and HF. After washing and sieving (15 μm), the residue was stored in deionized water.

3.3 New carbon-isotope analysis of total organic carbon and wood

Three hundred and forty-two (342) rock samples and 20 fossil wood samples were cleaned with deionized water to remove superficial impurities, then oven-dried at 40° and crushed in an agate mortar. The obtained powder was placed in a polypropylene Falcon tube and acid-washed with 10% HCl at least overnight, to remove carbonates. Residual powder was then rinsed with deionized water. $\delta^{13}C_{TOC}$ and $\delta^{13}C_{WOOD}$ analysis of the samples from the Dolomites (Italy) and the Transdanubian Range (Hungary) were carried out at the Department of Geosciences of the

University of Padova, Italy. $\delta^{13}C_{TOC}$ analyses of samples from the Julian Alps (Italy) were carried out at the Research Laboratory for Archaeology and the History of Art of the University of Oxford, UK. At the University of Padova, $\delta^{13}C_{TOC}$ analyses were performed on a Thermo Scientific Delta V Advantage Isotope Ratio Mass Spectrometer in continuous flow mode, coupled with a Flash 2000 Elemental Analyser and a ConFlo IV interface. Between 1 and 5 mg of sample were placed in a tin capsule and fed to the Elemental Analyser; the resulting CO_2 gas was analysed by the Mass Spectrometer. Blank correction was done on the base of a long-term mean of at least 30 tin cap analyses, and the results were calibrated against reiterated analyses of two international standards (IAEA-CH6, -10.449‰, and IAEA-CH7, -32.151‰). The long-term reproducibility, estimated on analyses of an internal standard (C3 plants sucrose), is better than 0.2‰ (1σ). At the University of Oxford, an aliquot of 10 mg of sample was analysed for $\delta^{13}C_{TOC}$ with a Carlo Erba nA 1108 Elemental Analyser combined with a SERCOn Geo 20/20 Isotope Ratio Mass Spectrometer running in continuous flow mode with a He carrier gas. The accuracy of isotope analyses (1σ = ±0.14‰) was calculated using an alanine in-house standard routinely checked against international standards IAEA-CH-6 and IAEA-CH-7 and traceable back to the V-PDB standard.

3.2 TOC and Rock-Eval pyrolysis

We quantified the Total Organic Carbon (TOC) of selected samples (n = 10) from Cave del Predil succession, and Rock-Eval pyrolysis was performed to quantify (mg HC/g of rock) the free hydrocarbons (S1) and the hydrocarbons that can be produced by thermal cracking of the kerogen (S2), to obtain information about the kerogen maturity (Tmax - °C) and quality (Hydrogen Index = S2*100/TOC; mg HC/g TOC). The instrument used was a Rock-Eval 6. The analyses were performed at Eni Upstream and Technical Services (San Donato Milanese, Italy). For TOC (%), 150–200 mg of ground rock samples were treated with HCl (9%) to remove carbonate minerals. The subsequent residue was washed with distilled water and the percentage of TOC in the sample measured using a LECO CS-200 carbon and sulphur analyser, heating the sample at high temperature in an oxygen stream (combustion). For Rock-Eval analysis, about 70–100 mg of ground rock were heated in a nitrogen atmosphere at 300°C for 3 minutes followed by a

programmed pyrolysis, increasing the oven temperature at 25°C/min to a final temperature of 550°C.

4. REVIEW OF THE BIOSTRATIGRAPHIC CONSTRAINTS

A robust stratigraphic correlation between the studied successions is possible using ammonoid, conodont, and sporomorphs biostratigraphy (Fig. 2). The pre-existing stratigraphy from the Dolomites (Italy) and the Transdanubian Range (Hungary) has already been published, to which the new data collected from the Julian Alps have been added. In this paper we follow a subdivision of the Julian into Julian 1, corresponding to the *Trachyceras* Zone (*Daxatina canadensis*, *Trachyceras aon*, and *Trachyceras aonoides* ammonoid subzones), and Julian 2, corresponding to the *Austrotrachyceras austriacum* ammonoid Zone (Fig. 1C; *sensu* Mietto *et al.*, 2012), and a subdivision of the Tuvalian into Tuvalian 1 (*Tropites dilleri* Zone), Tuvalian 2 (*Tropites subbullatus* Zone), and Tuvalian 3 (*Anatropites spinosus* Zone) (Fig. 1C; *sensu* Jenks *et al.*, 2015). This subdivision is slightly different than that used, for example, by Hornung *et al.*, 2007, where the Carnian is made up of three substages instead of two, and instead follows that already described by Dal Corso *et al.* (2015). In the following paragraphs the biostratigraphy of the studied successions are described in detail.

4.1 A revised biostratigraphy for Cave del Predil succession in the Julian Alps

Very few ammonoids were formerly known from the Raibl area in the Julian Alps. Suess (1867) and Stur (1868) collected ammonoids from “Raibl” that were later determined and illustrated by Mojsisovics (1882): *T. aon* from the Predil Limestone and two new species, *T. hacqueti*, and *T. roderici*, from a transitional facies between the Predil Limestone and the adjacent carbonate-platform slope. None of these specimens is still present in the museum collections at the Geologische Bundesanstalt, Vienna, Austria (I. Zorn, pers. comm.). However, the *T. aon* specimen was discussed by Urlichs (1994) and amended as *T. bipunctatum*. The new findings and newly determined specimens from museum collections from the Julian Alps are illustrated in Fig. 3 and include a rich ammonoid association from the Predil Limestone, and two specimens from the basal

Rio del Lago Formation. A few findings in the Predil Limestone may indicate the presence of the *T. aon* subzone, based on the occurrence of *T. muensteri* and *Brotheotrachyceras* sp., as well as the *T. bipunctatum* illustrated by Mojsisovics (1882) and amended by Urlichs (1994). Up to now these ammonoids have never been found higher than the *T. aon* subzone, but the distribution of ammonoids between the *T. aon* and *T. aonoides* subzones is still poorly constrained. Unfortunately, the boundary between these biozones is defined in the Prati di Stuores/Stuores Wiesen section in the Dolomites, Italy (Urlichs, 1974; 1994) between two horizons with a ca. 50 m intervening covered interval. It is therefore possible that ammonoids attributed to the uppermost *T. aon* subzone coexist with *T. aonoides* within this covered interval. Below the beds that yielded *T. muensteri* at Cave del Predil, *Sirenites cortinense* occurs, which is only known from the *aonoides* zone (Leonardi and Polo, 1952; Bizzarini, 2000); the distribution of the genus *Sirenites* is known to extend into the *A. austriacum* Zone (e.g., Krystyn, 1978; Lukeneder and Lukeneder, 2014). Above the horizon with *T. muensteri*, the rest of the Predil Limestone can be attributed to the *aonoides* zone, based on the presence of *Trachyceras pontius*, *T. saulus*, *T. cf. credneri* and *T. cf. velthemi*. The basal Rio del Lago Formation yielded *Neoprotrachyceras thous* and *Sirenites* sp., an ammonoid association that is typical of the *austriacum* zone, as illustrated by Krystyn (1978) and more recently by Lukeneder and Lukeneder (2014). The base of the *A. austriacum* Zone (base of the Julian 2) is thus close to the lithostratigraphic boundary between the Predil Limestone and the Rio del Lago Formation in the Cave del Predil (formerly “Raibl”) area of the Julian Alps.

In the lower part of the Tor Fm. the ammonoids *Neoprotrachyceras oedipus*, *Joannites* cf. *styriaca*, and *Proarcestes gaytani* indicate a Julian 2 age (De Zanche *et al.*, 2000; Roghi 2004, and references therein). The ammonoids found in the Cornitza Fm. (*Tropites subbullatus*, *Projuvites* sp., *Discotropites plinii*, *Gonojuvavites* sp.) allow dating of the the formation as Tuvalian 2 – Tuvalian 3 (De Zanche *et al.*, 2000).

Preliminary sporomorph biostratigraphic data from the lowermost part of the Rio del Lago Formation show an assemblage with *Aulisporites astigmosus*, *Equisetosporites chinleanus*, and *Vallasporites ignacii*. The presence of these forms allows placing of the boundary between the *Concentricisporites bianulatis* and *Aulisporites astigmosus* assemblages (*sensu* Roghi *et al.*, 2010)

357 at the base of the Rio del Lago Formation (Fig. 4), which is in agreement with the age given now
358 by the ammonoids. The sporomorph data of the Rio del Lago Formation do not allow the
359 *Aulisporites astigmosus* and *Lagenella martini* assemblages of Roghi *et al.* (2010) to be resolved.
360 In the Carnitza Fm., the *Granuloperculatipollis rudis* assemblage is defined by the appearance of
361 *Infernopollenites sulcatus*, cf. *Brodispora* sp., *Granuloperculatipollis rudis* and *Paracirculina*
362 *quadruplicis*. The age of this assemblage is calibrated by ammonoid biostratigraphy to the Tuvalian
363 2 – Tuvalian 3, i.e *Tropites subbullatus – Anatropites spinosus* Zones (Roghi 2004).
364 A monospecific fauna with the conodont species *Nicoraella? budaensis* was extracted from
365 the same samples that yielded the ammonoid species *Trachyceras pontius* (sample RF 205 44),
366 and *Trachyceras* cf. *humboldti* (sample RF 205 45) collected from the Predil Limestone (Fig. 5),
367 which are exclusive to the *T. aonoides* ammonoid subzone. The conodont *Nicoraella? budaensis*
368 was also collected from the Conzen and Tor Formations up to horizons close to the boundary with
369 the Portella Dolomite, along with *Nicoraella?* sp. A and *N.*? sp. B described by Kolar-Jurkovšek *et*
370 *al.* (2005) from the Raibl Beds of the Košuta Nappe in the western Karavanke Mts. (Slovenia) (Fig.
371 5). The genus *Nicoraella?* is a cavitate conodont mostly occurring in restricted-basin facies, as
372 both monospecific fauna and in mass occurrences, even though it has been found also in the
373 pelagic facies of Cozzo Paparino (Sicily), associated with *Gladigondolella* (Kozur and Mock, 1991).
374 Similarly to other Upper Triassic cavitate conodonts (e.g., *Misikella* spp.), the genus *Nicoraella?* is
375 found here in sediments deposited during an interval of climatic and environmental change, which
376 is associated with increasing temperatures (Trotter *et al.*, 2015). In particular, a monospecific fauna
377 of *Nicoraella? budaensis* was collected in the second of the three clastic horizons (mainly shale
378 and marlstone; “Raibl beds”) of the Mežica area, Karavanke Mts. (Slovenia) (Kolar-Jurkovšek and
379 Jurkovšek, 2010), which were deposited during the CPE, and correlates with the Tor Formation in
380 the Julian Alps (Roghi et al., 2010). A revision of the conodonts illustrated in Lieberman (1978)
381 improved the dating of the Carnitza Formation. The species illustrated in Fig. 1a, b of Lieberman
382 (1978) is clearly the long-ranged taxon *Paragondolella polygnathiformis*, which had its first
383 appearance at the base of the Julian and disappeared in the mid-Tuvalian. The other specimens
384 illustrated in Fig. 2 a, b of Lieberman (1978) are re-determined here as *Carnepigondolella zoae*, a

typical Tuvalian species. The stratigraphic ranges of these two species have only a short interval of overlap in the lower–middle Tuvalian (Rigo *et al.,* 2018). Therefore, the fossil fauna and microflora found in the studied succession of the Julian Alps allow definition of the biozones as illustrated in Fig. 2.

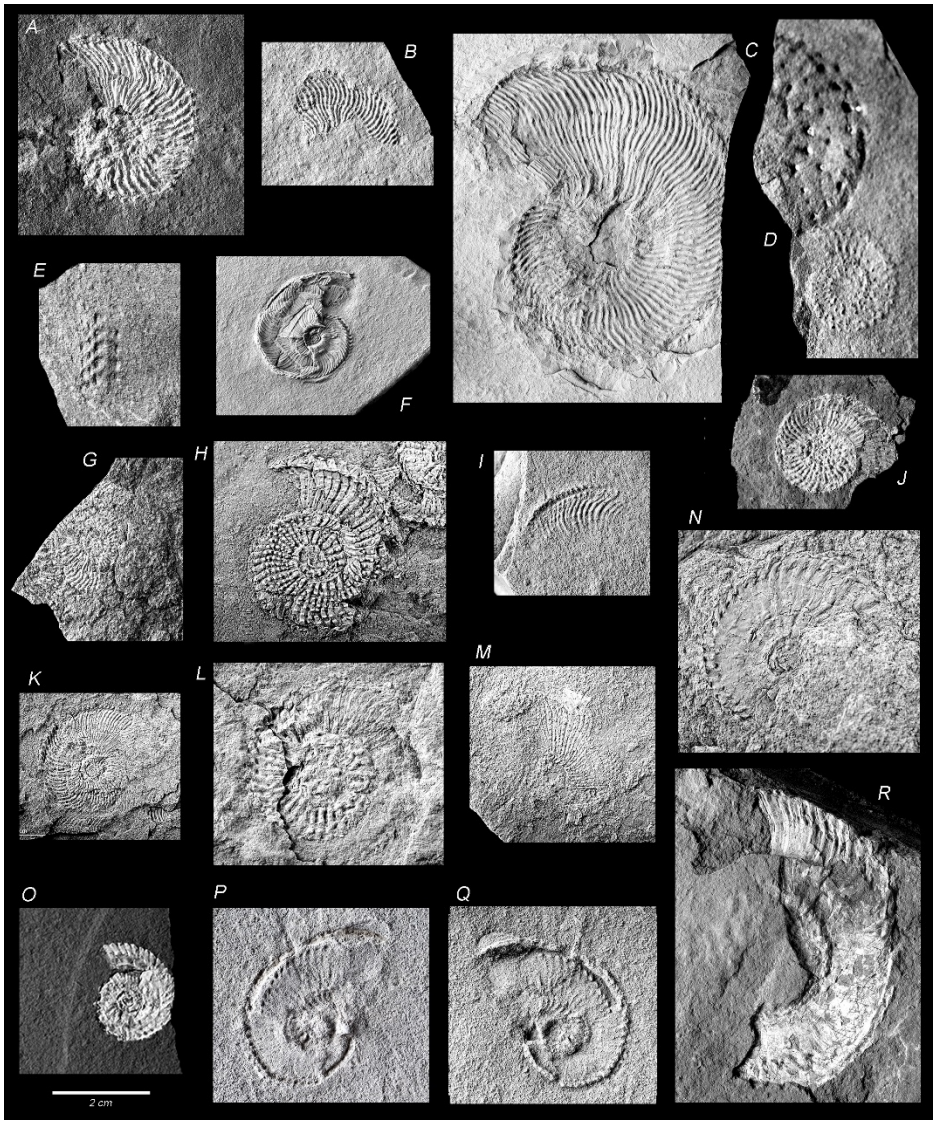

Figure 3. Ammonoids from the Cave del Predil succession (Julian Alps, Italy). A) *Brotheotrachyceras* sp. Sample PRAS 1.12; Rio Prasnig section, *T. aon-aonoides* subzones. B) *Trachyceras muensteri* Wissmann 1841. Sample CAPR 15.1; Cave del Predil section, *aon-aonoides* subzones. C) *Trachyceras bipunctatum* Münster 1834. Sample GBA 2017/036/0001; Raibl; *aon-aonoides* subzones. D) *Sirenotrachyceras* cf. *furcatum* Münster 1841. Sample PSG 1A.3; Rio Prasnig section; *aon-aonoides* subzones. E) *Sirenotrachyceras* cf. *furcatum* Münster 1841. Sample PSG 8B.1 (ventral view); Rio Prasnig section; *aon-aonoides* subzones. F) *"Paratrachyceras" jaegeri* Klipstein 1843. Sample MFSN 44151; Rio Klinken; *aon-aonoides* subzones. G) *Trachyceras* cf. *credneri* Klipstein 1843. Sample RF 204.1; Rio Prasnig section; *aonoides* Subzone. H) *Trachyceras humboldti* Klipstein 1843. Sample RF 205.42a; Rio Prasnig section; *aonoides* Subzone. I) *Trachyceras humboldti* Klipstein, 1843. Sample PRAS 1.8; Rio Prasnig section; *aonoides* Subzone. J) *Trachyceras* cf. *medusae* Mojsisovics in Wöhrmann 1889. Sample MFSN44161.5; Rio Prasnig; *aonoides* subzone. K) *Trachyceras pontius* Laube 1869. Sample RF 206.1b; Rio Prasnig section; *aonoides* Subzone. L) *Trachyceras saulus* Laube 1869. Sample RF 206.1a; Rio Prasnig section; *aonoides* subzone. M) *Trachyceras* cf. *velthemi* Klipstein 1843. Sample RF 204.4; Rio Prasnig section; *aonoides* subzone. N) *"Diplosirenites" hacqueti* Mojsisovics 1882. Sample RPG 2.3b; Rio Prasnig section; *aonoides* subzone. O) *"Diplosirenites" hacqueti* (Mojsisovics, 1882). Sample MFSN44155.2; Rio Prasnig section; *aonoides* Subzone. P) *Sirenites cortinense* Leonardi & Polo, 1952. Sample CAPR 16.2a (negative); Cave del Predil section; *aonoides* Subzone. Q) *Sirenites cortinense* Leonardi & Polo 1952. Sample CAPR 16.2b (positive); Cave del Predil section; *aonoides* Subzone. R) *Neoprotrachyceras thous* (Dittmar, 1866). Sample MPCM 7773; Rio Prasnig section; *A. austriacum* Zone.

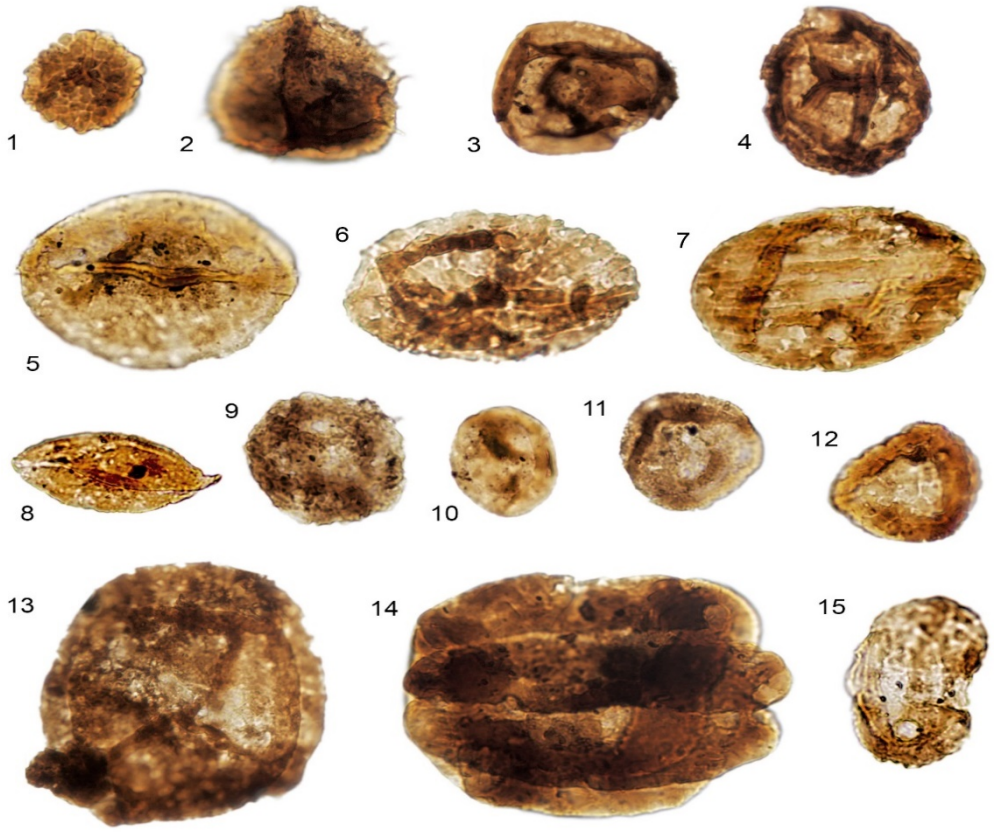

Figure 4. Sporomorphs from the Rio del Lago Formation (Cave del Predil, Julian Alps, Italy). 1) *Uvaesporites* sp., diameter 29 µm; RCB3 II, L32; 2) *Kraeuselisporites* sp., diameter 48 µm; RCB II, Q37. 3) *Aulisporites astigmosus*, diameter 56 µm, RCB3 II, M23/2. 4) *Aulisporites astigmosus*, diameter 51 µm, RCB3 I, E31. 5) *Aratrisporites scabratus*, wide 67 µm, RCB3 I, J41. 6) *Equisetosporites chinleanus*, height 73.6 µm, width 44.8 µm, RCB2 I, E25/4. 7) *Equisetosporites chinleanus*, height 70 µm, width 50 µm, RCB2 I, G54. 8) *Cycadophites* sp., higth 52 µm, RCB3 II, E25. 9) Vallasporites ignacii, diameter 40 µm, RCB3 II, o19. 10) *Paracirculina maljawkinae*, diameter 32 µm, RCB3 II, E30/4. 11) *Duplicisporites granulatus*, diameter 35 µm, RCB3 II, Q29/3. 12) *Duplicisporites verrucatus*, diameter 35 µm, RCB3 II, T30/3. 13) *Concentricisporites* sp., diameter 56 µm, RCB3 I, K36/2. 14) *Infernopollenites sulcatus*, width 96 µm, RCB3 I, E33/3. 15) *Luekysporites* sp., width 33.6 µm, RCB3 II, G20/4.

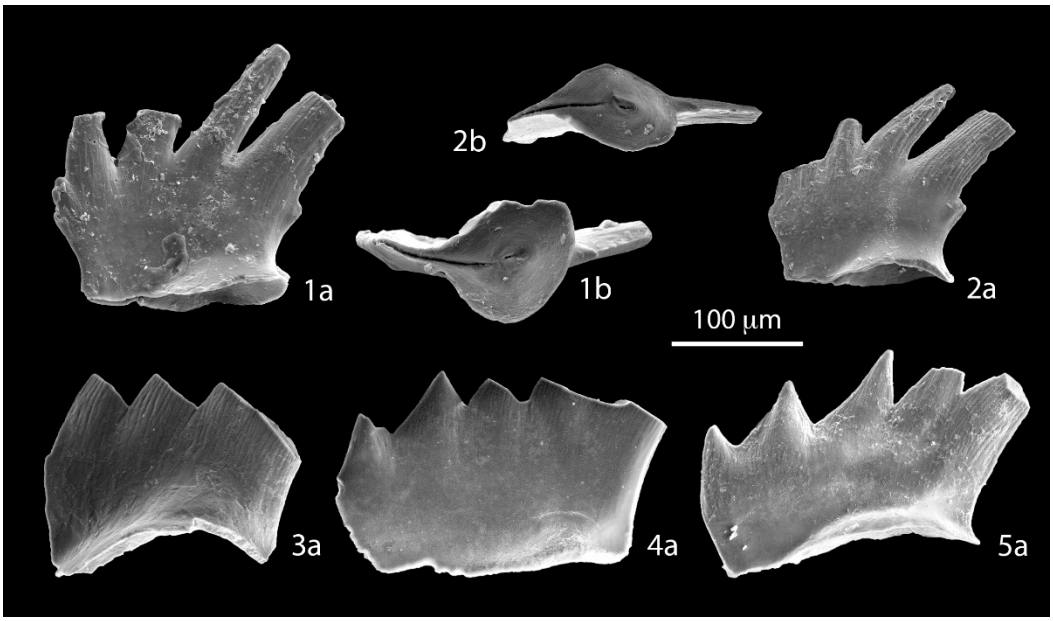

Figure 5. Scanning Electron Microscope photomicrographs of conodont specimens. 1) *Nicoraella? budaensis*, sample RF 205 44; 2) *Nicoraella? budaensis*, sample RF 205 45; 3) *Nicoraella n. sp. A* sensu Kolar-Jurkovšek *et al.* (2005), sample PORC 4bis; 4,5) *Nicoraella sp. B* sensu Kolar-Jurkovšek *et al.* (2005), sample PORC 12. For each specimen: (a) lateral view, (b) lower view. Scale bar 100 µm. Colour Alteration Index = 1.5.

443 **4.2 Dolomites: Overview of the published data**

444 The biostratigraphy of the Dolomites has been summarized in Breda *et al.* (2009) and Dal Corso *et*
445 *al.* (2015). At Milieres (Fig. 6), within the lowermost Heligkreuz Fm., it is possible to define the
446 Julian 1–Julian 2 boundary by the contact between the *Concentricisporites bianulatus* and
447 *Aulisporites astigmosus* sporomorph assemblages. The *Aulisporites astigmosus* assemblage is
448 characterized by the co-occurrence of *Aulisporites astigmosus*, *Aratrisporites* spp., *Calamospora*
449 *lunzensis*, *Kraeuselisporites cooksonae*, *Distalanulasporites punctus*, *Leschikisporis aduncus*,
450 *Tigrisporites halleinis*, *Duplexisporites* sp. 1 (Roghi *et al.*, 2010). Bizzarini and Braga (1987) found
451 ammonoids of the *Austrotrachyceras* zone in the uppermost part of the Milieres section, which are
452 associated with the sporomorphs of the *Aulisporites astigmosus* assemblage (Roghi *et al.*, 2010;
453 Fig. 2). Julian conodonts (*Paragondolella auriformis*, *Paragondolella polygnathiformis*,
454 *Gladigondolella tethydis*, *Gladigondolella m. malayensis*) are present in the lowermost Heligkreuz
455 Fm. (Mastandrea, 1994). Hence, on the basis of ammonoid, conodont and sporomorph
456 biostratigraphy, the Julian 1–Julian 2 boundary can be placed as in Fig. 2 and Fig. 6. In the Borca
457 Mb. of the Heiligkreuz Fm. (Fig. 2; Dibona section) the ammonoids *Austritrachyceras* sp. and
458 *Sirenites senticosus* have been found and give a Julian 2 age (Breda *et al.*, 2009). In the Dibona
459 Mb. of the Heiligkreuz Fm., the *Lagenella martini* sporomorph assemblage is present (e.g., spores
460 as *Baculatisporites comaumensis*, *Combaculatisporites mesozoicus*, *Leschikisporites aduncus*,
461 *Raistrickia alpina*, and pollen such as *Lagenella martinii*, *Equisetosporites chinleanus*,
462 *Araucariacites australis* and *Araucariacites* cf. *A. fissus*) (Fig. 2; Roghi *et al.*, 2010). The *Lagenella*
463 *martini* assemblage is calibrated with ammonids and conodonts in the Dolomites and in the
464 Northern Calcareous Alps (Raibler Schichten; Austria): its range goes from the Julian 2 to the base
465 of the Tuvalian 2 (Roghi *et al.*, 2010; Maron *et al.*, 2017). In the succession of the Dolomites, the
466 *Lagenella martini* assemblage is indeed found up to the Lagazuoi Mb. of the Heiligkreuz Fm. (Fig.
467 2) together with the ammonoids *Shastites* cf. *pilari* and cf. *Jovites* sp., and with the conodonts *P.*
468 *noah* and *Metapolygnathus praecommunisti*, which give a Tuvalian 1 age (Breda *et al.*, 2009;
469 Maron *et al.*, 2017). The Julian–Tuvalian boundary in the Dolomites is placed in the uppermost
470 Dibona Mb. of the Heiligkreuz Fm., where Tuvalian ammonoids occur. The Travenanzes Fm. is

dated to the Tuvalian 2 by the presence of a *Granuloperculatipollis rudis* sporomorph assemblage, which in the Julian Alps is calibrated to the Tuvalian 2–Tuvalian 3 by ammonoid biostratigraphy (see section 4.1 and Roghi 2004).

4.3 Transdanubian Range: Overview of the published data

Diagnostic ammonoids and conodonts, although rare, have been found in the Füred Limestone. *Frankites sp.* and *Trachyceras aon* are present and give a Julian 1 age (*Trachyceras* ammonoid Zone, Dosztály *et al.*, 1989; Kovács *et al.*, 1991; Budai *et al.*, 1999; Fig. 2). An early Julian age is also confirmed by the presence of the conodonts *Gladigondollela tethydis*, *Paragondolella foliata*, *Paragondolella foliata inclinata* (Fig. 2). In the uppermost part of the Füred Limestone the ammonoids *Neoprotrachyceras* spp. and *Sirenites* sp. have been found, and give a Julian 2 age (cf. Krystyn, 1983; Lukeneder and Lukeneder, 2013). The Julian 1–Julian 2 boundary is thus placed in the uppermost Füred Limestone (Fig. 2). In the Veszprém Marls, a rich ammonoid fauna with *Austrotrachyceras austriacum* is present in the Nosztor Limestone Member (also known as the *Austriacum* beds; Fig. 2). *Neoprotrachyceras baconicum* has been found in the Csicsó Member of the Veszprém Marls (Budai *et al.*, 1999; Dal Corso *et al.*, 2015). Therefore, the Veszprém Marls can be dated to Julian 2 (Fig. 2). This age-attribution is also confirmed by the presence of sporomorphs of the *Aulisporites astigmosus* assemblage (*sensu* Roghi et al., 2010) throughout the Veszprém Marls (Góczán et al., 1991) that, as in the Dolomites and the Julian Alps, are found in association with ammonoids of the Julian 2 (see above and Roghi et al., 2010). In the shallow-water Sándorhegy Formation, ammonoids have not been found, but sporomorphs biostratigraphy allows the Julian–Tuvalian boundary to be placed in the lowermost part of the formation, where Tuvalian pollen and spores appear (Góczán and Oravecz-Scheffer 1996; Budai et al., 1999; Fig., 2).

4.4 Biostratigraphic correlation of the studied sedimentary successions

On the basis of the new and published biostratigraphic data, a solid correlation between the successions of the Dolomites, Julian Alps, and Transdanubian Range can be traced at ammonoid-

zone resolution (Fig. 2 and Fig. 6). The upper San Cassiano Fm. can be correlated to the Predil Limestone of the Julian Alps and the Füred Limestone of the Transdanubian Range, which both have a Julian 1 age. The lower part of the Heiligkreuz Fm. of the Dolomites (Borca Member and most of the Dibona Member as in Fig. 6) has a Julian 2 age and can be correlated with the uppermost Predil Limestone, the Rio del Lago Formation, the Conzen Fm., and part of the Tor Fm. of the Julian Alps, and to the uppermost Füred Limestone, and the Veszprém Marls of the Transdanubian Range. The Julian–-Tuvalian boundary can be placed in the Dolomites in the uppermost Dibona Member of the Heilgkreuz Fm., and in the Transdanubian Range in the lowermost Sándorhegy Fm., which can be therefore correlated with each other. In the Julian Alps, the precise placement of the Julian–Tuvalian boundary is less easy, given the absence of diagnostic taxa belonging to the Tuvalian 1 (*Tropites dilleri* ammonoid Zone). However, ammonoids of the lowermost Carnitza Fm. are Tuvalian 2 in age (*Tropites subbullatus* ammonoid Zone; Fig. 2). Hence, the Julian–Tuvalian boundary must be placed between the uppermost Tor Fm. and the Portella Limestone, which gives the correlation with the Dolomites and the Transdanubian Range as shown in figure 2.

5. NEW CARBON-ISOTOPE AND ROCK-EVAL DATA

All $\delta^{13}C$ data of total organic matter and wood are given in Fig.6 and Supplementary Tables. $\delta^{13}C_{TOC}$ data from the Julian Alps show, at the base of the Rio del Lago Formation, a negative excursion of approximately 3‰ (NCIE-1). This excursion occurs at the Julian 1–Julian 2 boundary and, on the basis of the biostratigraphic constraints, can be robustly correlated to the shift already found in the Dolomites and Hungary (Fig. 6), Austria, Barents Sea and China at the onset of the CPE (Dal Corso *et al.*, 2015; Mueller *et al.*, 2016a, 2016b; Sun *et al.*, 2016).

In the Balaton Highland (Hungary) and in the Julian Alps (Italy), the $\delta^{13}C_{TOC}$ records show a second 3–6‰ negative carbon-isotope excursion within the Julian 2 interval (NCIE-2). This NCIE-2 occurs in the Mencshely Mb. of the Veszprem Marls in the Met-1 core of the Balaton Highland in Hungary, and in the Conzen Formation in the Cave del Predil succession of Julian Alps in Italy (Fig. 6). Rock-Eval pyrolysis analysis shows that the organic matter is Type-III (terrestrial)

527 throughout the NCIE-2 in the Julian Alps and is immature with respect to oil generation (Fig. 7).
528 The biostratigraphy of these units strongly supports the correlation of the NCIE-2 between the
529 Transdanubian Range and the Julian Alps (Fig. 6). Similarly, at the base of the Heiligkreuz section
530 (metres 0–5, Borca Mb.; Fig. 6) in the Dolomites (Italy), a positive shift of about 4‰ of Julian 2 age
531 is correlated to the positive rebound of the NCIE-2 recorded in the Balaton Highland and in the
532 Julian Alps.

533 A third negative $\delta^{13}C_{TOC}$ shift of approximately 4‰ (NCIE-3) occurs at the Julian–Tuvalian
534 boundary in the Dolomites (at metre 42.2 in the Heiligkreuz section and at metre 142.9 in the
535 Dibona section) and in the Zsámbék Basin (metre 340 of the Zs-14 core; Fig. 6). In the Dolomites
536 (Heiligkreuz section), wood collected from a level within the NCIE-3 has $\delta^{13}C_{WOOD}$ values lowered
537 by 2‰ with respect to wood collected from two levels below the NCIE-3 (Fig. 6). In the Dibona
538 section (Dolomites), the NCIE-3 rebounds to pre-excursion $\delta^{13}C_{TOC}$ values approximately at metre
539 175 at the base of the Travenanzes Formation (Fig. 6).

540 A fourth negative shift (NCIE-4) is recorded by bulk organic matter at the base of the
541 Travenanzes Fm., i.e., at the base of Tuvalian 2 approximately at metre 180 of the Dibona section
542 (Fig. 6). The NCIE-4 rebounds to pre-excursion values at approximately metre 220, to remain
543 relatively stable through the Travenanzes Fm. (Fig. 6). Similarly, in the Julian Alps, the carbon-
544 isotope values of bulk organic matter at the base of the Carnitza Fm. (base of the Tuvalian 2;
545 approx. metre 60 at Portella section; Fig. 6) are on average 1.5–2‰ lower than those at the top of
546 the Tor Fm. (metre 0–40 of the Portella section; Fig. 6).
547
548

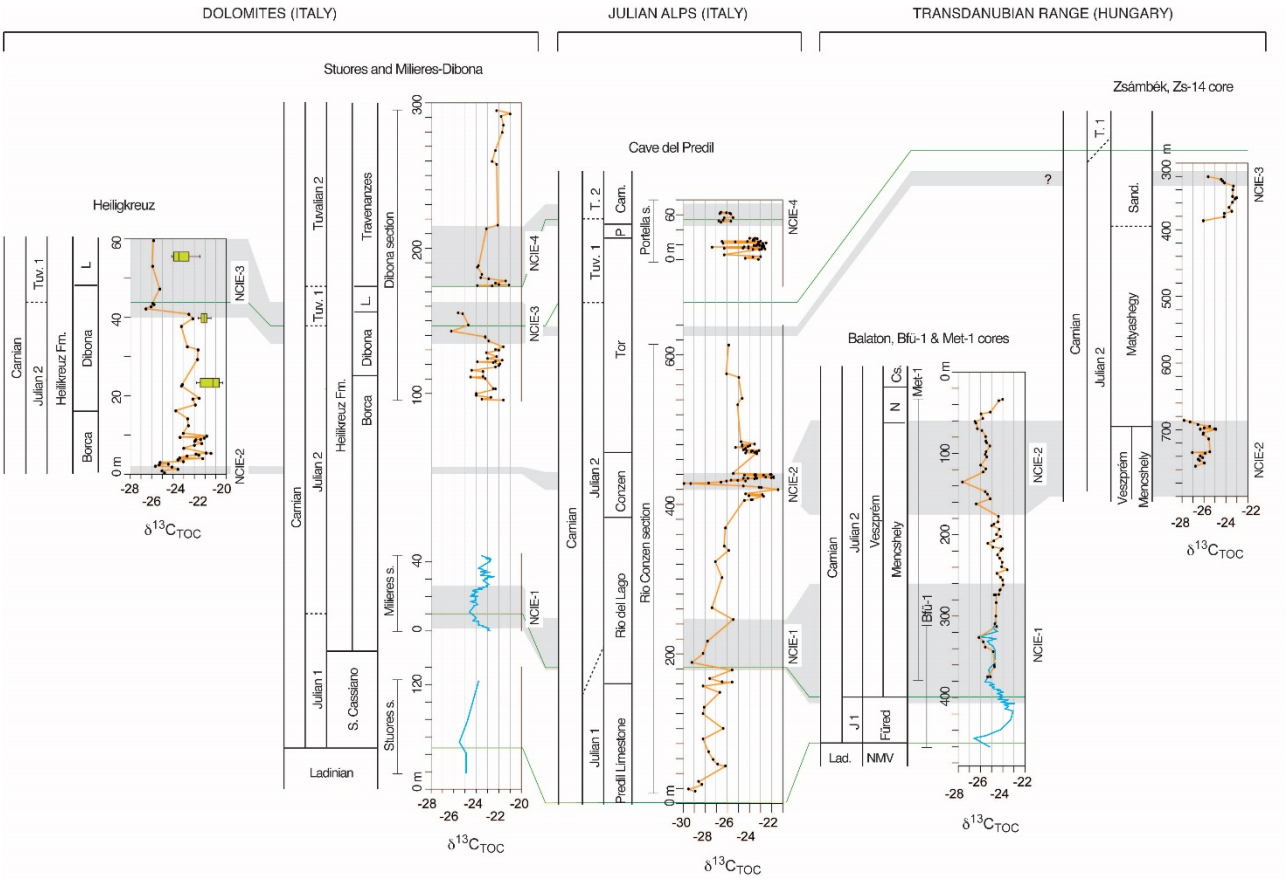

Figure 6. Total organic carbon-isotope ($\delta^{13}C_{TOC}$) records across the Carnian Pluvial Episode (Julian–Tuvalian) in Italy and Hungary. The black dots and orange lines are the organic carbon-isotope curves from the Dolomites (Dolomites succession), the Julian Alps (Cave del Predil succession) and the Transdanubian Range (Balaton and Zsámbék successions) produced in this study. Wood carbon-isotope data from the Heiligkreuz are represented as green box-and-whiskers plots. Light blue lines are published organic carbon-isotope curves from the Dolomites in Italy, and the Transdanubian Range in Hungary (Dal Corso *et al.*, 2012, 2015). The correlation (green lines) is based on biostratigraphic framework (ammonoid, conodont, and sporomorph data) given in detail in Fig. 2. The grey bars correlate the four negative carbon-isotope excursions (NCIEs) detected in this study. Raw carbon-isotope data are given in the Supplementary Tables.

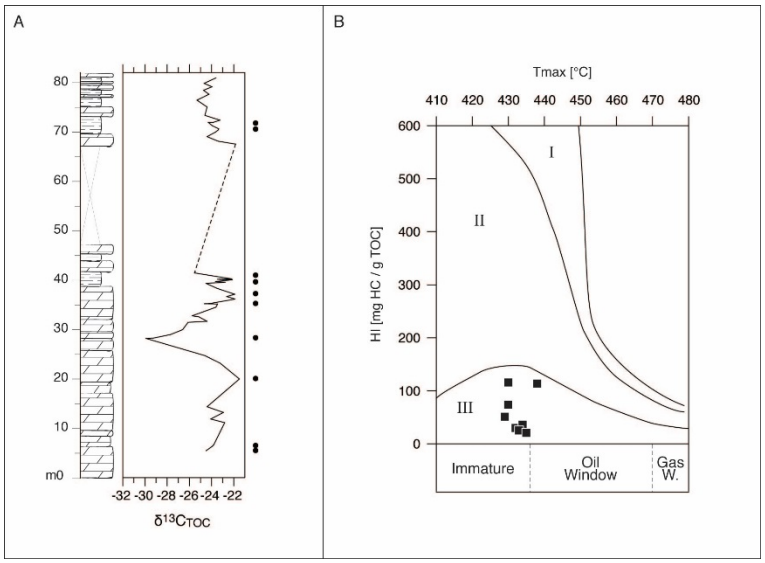

574
575
576
577 **Figure 7**. Rock-Eval pyrolysis data, Rio delle Cascate segment of the Cave del Predil succession. A)
578 Position of the samples analysed with Rock-Eval pyrolysis against the carbon-isotope data. Samples were
579 selected to encompass the NCIE-2 at Cave del Predil (see main text). B) Hydrogen Index (HI) *vs* Tmax. The
580 organic matter of the analysed samples is Type III, and immature with respect to oil generation. The well-
581 preserved palynological associations found in the same stratigraphic section (Roghi 2004) support the Rock-
582 Eval results, since the terrestrial elements (pollen and spores) are much more abundant than the marine
583 elements (acritarchs and algae).
584
585

6. DISCUSSION

6.1. Multiple carbon-isotope excursions punctuated the CPE

Miller *et al.* (2017) showed that not just one, but multiple CIEs are associated with the environmental perturbations that define the CPE in Europe. The Wiscombe Park Borehole studied by Miller *et al.* (2017) was drilled through a continental succession and its age can be defined by sporomorphs biostratigraphy. Sun *et al.* (2016) found one single, broad negative CIE in bulk organic matter during the CPE in a marine succession in South China, but the carbonate carbon-isotope record seems to record three negative CIE within the same interval. The age of the Chinese succession is constrained by conodont biostratigraphy and one ammonoid occurrence (Sun *et al.*, 2016). The new data from sections of the North-Western Tethyan realm show three, possibly four, sharp negative carbon-isotope excursions punctuating the CPE (Fig. 6) that can be dated biostratigraphically with ammonoids, conodonts and sporomorphs.

The NCIE-1 at the Julian 1–Julian 2 boundary (Fig. 6) has already been identified in different geological settings and in a variety of organic substrates as in $\delta^{13}C$ records of marine and terrestrial biomarkers (Dal Corso *et al.*, 2012), $\delta^{13}C$ records of total organic carbon (Dal Corso *et al.*, 2012, 2015; Mueller *et al.*, 2016a, 2016b; Sun *et al.*, 2016), and in $\delta^{13}C$ records of carbonate carbon (Muttoni *et al.*, 2014; Sun *et al.*, 2016). These shifts indicate an injection of ^{13}C-depleted carbon into the ocean–atmosphere system at the onset of the CPE. New data show that the NCIE-1 occurs also at the base of the Rio del Lago Formation of the Cave del Predil succession in the Julian Alps, where the Julian 1–Julian 2 boundary is placed according to ammonoid biostratigraphy. This new record shows that the NCIE-1 followed a long-term global positive $\delta^{13}C$ shift, as registered by both organic matter and brachiopod calcite in various geological settings (Korte *et al.*, 2005; Dal Corso *et al.*, 2011, 2012, 2015). This long-term rise in $\delta^{13}C$ has been explained as due to increased sequestration of ^{12}C linked to the spread of coal swamps, the remains of which were lost in the geological record after the Permian/Triassic mass extinction (Korte *et al.*, 2005).

At least three additional major negative $\delta^{13}C$ shifts followed the initial NCIE-1 of the CPE (Fig. 6). A 3–6‰ negative shift (NCIE-2) is recorded in the Hungarian series (Met-1 core), in the

614 Julian Alps (Cave del Predil), and partially in the Dolomites (Heiligkreuz section). It occurs in the *A.*
615 *austriacum* ammonoid Zone, i.e., the Julian 2 biochronozone (Fig. 6). Rock-Eval pyrolysis shows
616 that organic matter is immature with respect to oil generation across the NCIE-2 in the Julian Alps
617 (Fig. 7), and the low colour alteration index of conodont apatite between 1 and 1.5, and clay
618 mineralogy, suggest low burial temperatures in the successions of the Dolomites, Julian Alps and
619 Hungary (this study and Rostási *et al.*, 2011). Laboratory studies have shown that thermal
620 maturation produces either no change in the pristine $\delta^{13}C$ value of organic matter or small levels of
621 ^{13}C-enrichment (Lewan, 1983; Galimov, 2006). Major changes occur only during late diagenetic
622 and metamorphic stages. For example, ^{13}C-enrichment of 1–2‰, caused by a more rapid breaking
623 of ^{12}C-^{12}C with respect to others C-C bonds, was observed in shales and coals at the contact with
624 magmatic intrusions (McKirdy and Powell, 1974; Simoneit *et al.*, 1978; Saxby and Stephenson,
625 1987). Hence, thermal maturation could not have been responsible for the observed changes in
626 $\delta^{13}C$ of the bulk organic matter. Rock-Eval pyrolysis shows also that the analysed organic matter is
627 type III in the Julian Alps, i.e., mainly terrestrial in origin, across the entire NCIE-2 (Fig. 7), this
628 being confirmed also by the rich and well-preserved palynological associations found in the same
629 stratigraphic interval, where pollen and spores (terrestrial) are the most abundant elements while
630 acritarchs and algae (marine) are very rare (Roghi 2004). Therefore, changes in the source of the
631 organic matter (marine *vs* terrestrial) cannot account for the recorded $\delta^{13}C$ excursion (see also
632 6.2). The synchronous occurrence of the NCIE-2 in different geological settings suggests it
633 represents a genuine change in the global carbon-isotope composition of organic matter. We thus
634 propose that the NCIE-2 represents a shift in the isotopic composition of the ocean–atmosphere
635 system within the Julian 2 interval (*A. austriacum* ammonoid Zone).
636 In the Dolomites (upper part of the Heiligkreuz Fm. of the Dibona and Heiligkreuz sections),
637 the organic matter records a 4‰ $\delta^{13}C_{TOC}$ negative shift at the Julian–Tuvalian boundary. This shift
638 is labelled as NCIE-3 in Fig. 6. This shift is recorded clearly by bulk organic carbon, but it also
639 occurs in wood; the $\delta^{13}C_{WOOD}$ from the Heiligkreuz section shows shifts of about -2‰ in
640 correspondence with the NCIE-3 (Fig. 6). The onset of the NCIE-3 is also visible in Hungary at the
641 very top of the studied core (Zs-14), within the Sandorhegy Fm. (Fig. 6). In the Dolomites (Milieres-

642 Dibona section), the colour alteration index of conodont apatite is very low (1; Preto *et al.*, 2015),
643 and previous biomarker analysis of organic matter showed the succession experienced negligible
644 thermal maturation (Dal Corso *et al.*, 2012). For the reasons outlined above, diagenesis cannot be
645 considered the cause of the observed negative shift in the $\delta^{13}C_{TOC}$. Moreover, the fact that wood
646 recorded a similar shift strongly suggests a negative excursion in the carbon-isotope composition
647 of the atmosphere. This supposition is supported by the fact that changes in the carbon-isotope
648 composition of wood are similar to those in marine carbonates and organic matter, and therefore
649 represent a good proxy for the carbon-isotope composition of the palaeoatmosphere (e.g. Gröcke
650 et al., 1999; Hesselbo *et al.*, 2007; Dal Corso *et al.*, 2011). Thus, the concurrent shifts in the
651 geochemical signatures of total organic carbon and wood strongly suggests that NCIE-3
652 represents a change in the carbon-isotope composition of the Carnian ocean–atmosphere system
653 towards more ^{13}C-depleted values.
654 A possible 1.5–2‰ NCIE-4 could be present at the base of the Travenanzes Fm. (base of
655 the Tuvalian 2) in the Dibona section (Dolomites, Fig. 5). Unfortunately, no wood has been found in
656 this portion of the Dibona section to support the total organic carbon-isotope data. The NCIE-4
657 recorded at Dibona can be stratigraphically correlated to a similar NCIE recorded in the Portella
658 section of the Julian Alps (Fig. 2 and Fig. 5), a correlation supported by sporomorph and
659 ammonoid biostratigraphy (De Zanche *et al.*, 2000; Roghi 2004; Preto *et al.*, 2005; Roghi *et al.*,
660 2010). More data are needed to confirm the global nature of the NCIE-4.
661
662 **6.2 Discrepancies in the magnitudes of the negative $\delta^{13}C_{TOC}$ excursions**
663 The new and published carbon-isotope curves across the sediments of the CPE show that each of
664 the NCIEs may have different magnitudes in different geological settings (Fig. 6). Dal Corso *et al.*
665 (2015) already pointed out this discrepancy by comparing the magnitudes of the NCIE-1 recorded
666 by TOC in the Dolomites (Italy), Northern Calcareous Alps (Austria), and Transdanubian Range
667 (Hungary), which range from 4‰ to 1.5‰ in total organic matter (Dal Corso *et al.*, 2012; 2015;
668 Mueller *et al.*, 2016a, 2016b; Miller *et al.*, 2017; this study), while the magnitude of the first shift is
669 more consistently around 3–4‰ when measured on leaf waxes *n*-alkanes (Dal Corso *et al.*, 2012;

Miller *et al.*, 2017). Such a pattern suggests that for the NCIE-1 the differences could be linked to local changes in the source of the organic carbon, i.e. shifts in the proportion of marine *vs* terrestrial organic matter in the marine sediments and/or changes in the marine and terrestrial community structure (Dal Corso et al., 2015). The same factors could apply equally for the other NCIEs that mark the entire CPE (Fig. 6).

The $\delta^{13}C$ signature of terrestrial and marine organic carbon depends on a number of factors such as the source when fixed during photosynthesis by primary producers, the photosynthetic pathway used to fix the carbon, and the environmental conditions (e.g. Diefendorf *et al.*, 2010; Dal Corso *et al.*, 2017). These issues explain why organic substrates have large carbon-isotope variability, as shown also for Carnian plant remains (Dal Corso *et al.*, 2011). Today, the $\delta^{13}C$ of terrestrial plants is on average more ^{13}C-depleted than that of marine algae but there is evidence that before the Cretaceous marine organic carbon, in many instances, was more ^{13}C-depleted than terrestrial carbon (Arthur *et al.*, 1985). This difference is also evident from our data: wood in the shallow-marine Heiligkreuz Fm. shows on average more positive $\delta^{13}C$ values than TOC, which likely has a marine organic-carbon component (Fig. 2). Therefore, an increase of terrestrial carbon into the Triassic marine basins could have resulted in a shift of the $\delta^{13}C_{TOC}$ toward more positive values. If this input of terrestrial organic carbon was coincident with a NCIE, the effect would have been an apparent attenuation of the NCIE itself, i.e., the magnitude of the NCIE recorded in marginal marine sediments would have been less than the shift in the atmosphere and in the oceans. One of the most striking characteristics of the CPE in the studied successions is the arrival into the basins of huge amounts of siliciclastic sediment. Since the NCIEs described in this work are associated to such inputs of siliciclastic sediments from land (see section 6.5), this effect could explain the differences observed in their magnitudes, depending on the distance from the coast and on the catchment area (Dal Corso *et al.*, 2015).

Other possible causes that could have contributed in modulating the $\delta^{13}C_{TOC}$ during the CPE are changes in the structure of the terrestrial and marine communities, and/or modifications in carbon-isotope fractionation during photosynthesis linked to variable environmental conditions. For example, it has been shown that the NCIEs at the Triassic–Jurassic boundary are correlated to the

relative abundance of different sporomorph taxa, which likely had different $\delta^{13}C$ signatures (Van de Schootbrugge *et al.*, 2008). In higher plants, carbon-isotope fractionation increases with increasing mean annual precipitation and increasing pCO_2 (Diefendorf *et al.*, 2010; Schubert and Jahren, 2012; Kohn, 2016). The magnitude of the NCIE-2 recorded in the Julian Alps (approx. 6‰; Fig. 6), for example, could have been amplified due to increasing higher-plant carbon-isotope fractionation, given that the organic carbon is mainly terrestrial in origin (Fig. 7) and was produced under the more humid climate conditions of the CPE. On the contrary, the NCIE-1 has a similar magnitude in both terrestrial and marine biomarkers, thus ruling out the possibility that a change in the terrestrial plant isotopic fractionation influenced the magnitude of the shift recorded by $\delta^{13}C_{TOC}$ (Dal Corso *et al.*, 2012; Dal Corso *et al.*, 2015).

The $\delta^{13}C$ of organic matter is controlled by many physiological and environmental factors, which can only be constrained with difficulty, especially in deep time (e.g., Dal Corso et al., 2017, and references therein). This fact leaves a certain degree of uncertainty in the interpretation of the carbon-isotope shifts recorded by the bulk organic matter. This complication is for example particularly relevant when mass-balance calculations are attempted on the basis of the magnitude of the $\delta^{13}C$ shifts in order to calculate the amount of ^{13}C-depleted C that has been transferred into the atmosphere and the ocean at the time of major climate perturbations in Earth's history. In the case of the CPE, however, the synchronous biostratigraphically-constrained occurrence of the NCIEs in different geological settings, the fact that some of these NCIEs are recorded by different organic substrates (wood, leaf-wax *n*-alkanes, and marine algal biomarkers), and the little or no diagenetic overprint on the analysed sediments, together strongly suggest that the shifts represent an actual change in the carbon-isotope composition of the Carnian ocean–land–atmosphere system.

6.3 Global correlation of the Carnian carbon-isotope excursions

Based on the biostratigraphic data, the carbon-isotope curves of the western Tethys realm have been tentatively correlated to the curves of the continental succession of Devon (Miller *et al.*, 2017), and of the Nanpanjiang Basin, Guizhou (South China Block; Sun *et al.*, 2016).

A correlation between the NCIEs recorded in this study and those found in the Carnian sediments from the WP borehole 1 (Devon, UK) by Miller *et al.* (2017) is not straightforward. The cored material from Devon in UK is a terrestrial succession of mudstone and siltstones, which represents a sabkha–lacustrine environment, whose age is constrained by sporomorph biostratigraphy. Sporomorphs give a Julian 1–Julian 2 age (Miller *et al.*, 2017), which is difficult to compare with the higher biostratigraphic resolution of this study provided by the integrated records of ammonoids, conodonts, and sporomorphs. However, the continental succession shows four distinct major NCIEs recorded by both bulk organic matter and higher-plant *n*-alkanes (Fig. 8; Miller *et al.*, 2017). In the upper part of the WP borehole 1 the circumpollen *P. quadruplicis* (Schuuring 1970) appears at metre 52 (supplementary material of Miller *et al.*, 2017). In the Southern Alps, where the sporomorph assemblages can be calibrated with ammonoid biozones, the first occurrence of *P. quadruplicis* is dated to the Tuvalian 2 (van der Eem, 1983; Roghi 2004; Roghi *et al.*, 2010). Moreover, Miller *et al.* (2017, their supplementary materials) interpreted the palynological association found in the uppermost part of the WP1 borehole as the *Lagenella martini* assemblage defined by Roghi *et al.* (2010). The portion of the core in which the *Lagenella martini* assemblage is found comprises the third and fourth NCIEs of Miller *et al.* (2017), i.e. from metre 56 of the WP borehole 1 above. The *Lagenella martini* assemblage is calibrated with ammonoids and extends from the uppermost Julian 2 to the Tuvalian 1 (see Fig. 9 of Roghi *et al.*, 2010). In the Dolomites, for example, a typical sporomorph association of the *Lagenella martini* assemblage is found in the Lagazuoi member of the Heiligkreuz Fm. together with Tuvalian ammonoids (*Shastites* cf. *pilari*). Hence, according to this interpretation, the pollen record at Wiscombe Park could indeed extend into the Tuvalian (Upper Carnian). Therefore, the NCIEs of Miller *et al.* (2017) could correlate to those found in this study as shown in Fig. 8. If this correlation were to be confirmed by future refined stratigraphic studies of the continental succession of Devon, it would imply that the entire CPE interval punctuated by the NCIEs, i.e., from the base of the Julian 2 to the base of the Tuvalian 2, lasted for ca. 1 Myrs (Fig. 8).

Sun *et al.* (2016) identify only one prolonged NCIE in the total organic matter of the Wayao Fm., (Nanpanjiang Basin, Guizhou, South China Block). This CIE begins at the base of Julian 2

754 and terminates within the Tuvalian 2. The carbonate carbon-isotope record, however, shows three
755 NCIEs. The differences between the carbonate and organic carbon-isotope records have been
756 explained by changes in the composition of the organic carbon deposited in the basin. The
757 correlation of each negative CIE in the carbonates of the Nanpanjiang Basin is, however, again not
758 straightforward, because of uncertainties on the age attributions. The conodonts illustrated by Sun
759 *et al.* (2016) include long-ranging species, i.e., *Paragondolella polygnathiformis* and *P. praelindae*,
760 occurring with a typical Julian association in the lower part of the section represented by
761 *Paragondolella foliata*, *P. inclinata* and *P. tadpole*. In the uppermost part of the section, the same
762 long-ranged taxa instead co-occur with a Tuvalian conodont association consisting of
763 *Paragondolellla noah* and *Hayashiella carpathica*. However, in this locality, *Paragondolella*
764 *noah* also occurs together with the typically Julian conodonts *P. foliata*, *P. inclinata* and *P. tadpole*.
765 The lowest occurrence of *P. noah* in Long Chang is to be dated to the Julian also because of the
766 ammonite *Austrotrachyceras* cf. *A. austriacum* found some 12 m above. This distribution is
767 unusual, because *P. noah* has hitherto only been documented in Tuvalian beds in both Tethyan
768 and Panthalassic region (e.g., Mazza *et al.*, 2012a; Orchard, 2014; Rigo *et al.*, 2017). Sun *et al.*
769 (2016) place the Julian–Tuvalian boundary close to the second negative shift in $\delta^{13}C_{CARB}$, which
770 would thus correspond to the NCIE-3 detected in the Southern Alps of Italy (this study) and,
771 possibly, with the third shift recorded in the WP borehole 1 from Devon (Miller et al., 2017) (Fig. 8).
772 It is more difficult to place the boundary between Tuvalian 1 and 2 in the Long Chang section. The
773 conodont species *P. noah* and *H. carpathica* first occur, in western Tethys, below the appearance
774 of the cosmopolitan species *Metapolygnathus praecommunisti* (Mazza *et al.*, 2011; Orchard, 2014;
775 Rigo et al., 2017), which is Tuvalian 1 (Fig. 2; Maron *et al.*, 2017). Conodonts become endemic
776 and rare in the Wayao Fm. of the Nanapanjiang Basin, thus complicating further subdivisions of the
777 Tuvalian at a regional scale (Sun *et al.*, 2016). Following the age attributions of Sun *et al.* (2016),
778 we correlated the NCIE-4 with the third carbonate carbon-isotope negative shift. However, we note
779 that the absence of *M. praecommunisti* may indicate a Tuvalian 1 age of the upper portion of the
780 Long Chang section and the absence of the Tuvalian 2. The NCIE-1 and the NCIE-2, as defined in
781 this study, are not resolved in the Long Chang section (Fig. 8). The biostratigraphically based

correlation of the successions of the North-western Tethys with that of Guizhou again supports the hypothesis that the entire CPE interval punctuated by the NCIEs lasted for ca. 1 Myr. Indeed, cyclostratigraphic study of an incomplete succession of the Xiaowa (=Wayao) Fm. in the Nanapanjiang Basin (South China) shows the CPE encompasses almost two 405-kyr cycles (Zhang *et al.*, 2015).

A record of stable carbon isotopes that contains multiple shifts was obtained by Mueller *et al.* (2016b) from bulk organic matter of marginal marine successions in Spitsbergen (Norway), which was part of the Boreal realm in the Late Triassic. These authors identified three NCIEs, dated on the base of palynostratigraphy and magnetostratigraphy near the Ladinian–Carnian boundary, at the base of the Julian 2 biochronozone (lower Carnian) and at the boundary between Tuvalian 2 and Tuvalian 3 biochronozones in the upper Carnian. Mueller *et al.* (2016b) suggest that all three shifts are present in the carbon-isotope record of Korte *et al.* (2005). Despite the richer palynological associations with respect to the WP borehole 1, which allowed a more accurate biostratigraphic dating of the NCIEs of Spitsbergen, a correlation with our new record from western Tethys is again not straightforward. A negative CIE at the Ladinian–Carnian boundary is actually not documented at Spitsbergen, where $\delta^{13}C$ values instead increase steadily from the Ladinian to the lower Carnian. Mueller *et al.* (2016b) correlated their stable-isotope data from Spitsbergen to the carbonate and bulk organic-matter $\delta^{13}C$ records from Tethys of Korte *et al.* (2005) and Dal Corso *et al.* (2015), and reinterpreted these latter datasets as containing the evidence of a negative carbon-isotope excursion at the Ladinian–Carnian boundary. This interpretation differs, however, from those of the original works. Mietto *et al.* (2012) did not identify any significant carbon-isotope change in the bulk carbonate at the Carnian GSSP. Mueller *et al.* (2016b) suggest that two stratigraphic intervals at the base of Julian 2 and between Tuvalian 2 and Tuvalian 3 stand out as prominent NCIEs. There is, however, a large and continuous variability in this record, which oscillates in a wide range from ca. -31‰ to -24‰ VPDB throughout the Carnian. It could be hypothesized that up to 5 NCIEs are present in the records from Spitsbergen, similarly to what has been found in Dorset (Miller *et al.*, 2017) and in Western Tethys (this work), but due to

809 an insufficient sampling resolution, the correct stratigraphic position of these excursions cannot not

810 be determined.

811

812

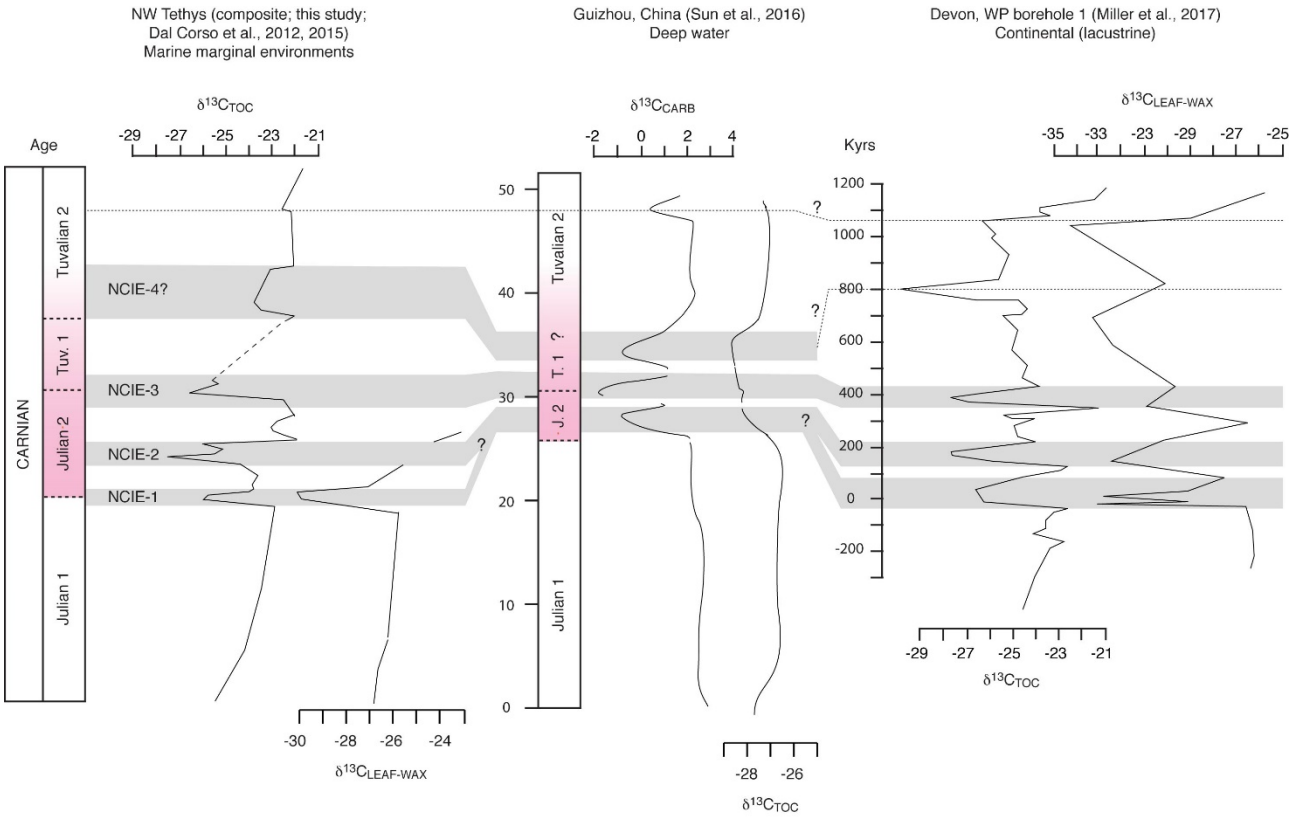

Figure 8. Chemostratigraphic correlation of the carbon-isotope records from the marine marginal successions of the north-western Tethyan realm (this study) and China (Sun *et al.*, 2016), and the lacustrine succession of Devon (WP borehole 1, UK; Miller *et al.*, 2017). The stylized organic carbon-isotope curve for the Western Tethys (this study) is drawn according to the data presented in Fig. 6 and summarized in Fig. 9 (raw data in the Supplementary Materials). Note that although the correlation of the records from the north-western Tethys and China with that from Devon is tentative and not sufficiently supported by biostratigraphic constraints, the records show similar distinct major carbon-isotope excursions in total organic matter (TOC) and leaf-wax *n*-alkanes. Sporomorphs from the WP borehole 1 give a Carnian (Julian–Tuvalian) age but do not allow a higher resolution biostratigraphic zonation of the units (Miller *et al.*, 2017). The duration of the WP borehole 1 interval containing the NCIEs has been estimated using gamma-ray and elemental abundance cyclicity (Miller *et al.*, 2017). The north-western Tethyan stylized curve is composite and thus the vertical scale does not reflect the actual thickness of the sedimentary successions (see Fig. 6 for the thickness of each studied sections). $\delta^{13}C_{LEAF\text{-}WAX}$ is expressed as weighted mean of odd C25-C31 *n*-alkanes (from Dal Corso *et al.*, 2012, Dolomites, and Miller *et al.*, 2017, Devon). The age of the Carnian Pluvial Episode is shown in pink. J 2 = Julian 2, T 1 = Tuvalian 1.

837 **6.4 LIP volcanism as trigger of the carbon-isotope excursions**

838 Our new data show that three (possibly four) major negative excursions in the carbon-isotope
839 composition of the ocean–atmosphere system occurred during the CPE. The first NCIE is at the
840 Julian 1–Julian 2 boundary, the second within the Julian 2, the third at the Julian–Tuvalian
841 boundary, and a possible fourth may exist at the base of the Tuvalian 2 (Fig. 6). Given their close
842 ages, these repeated disruptions in the carbon cycle could have been related to the emplacement
843 of large masses of volcanic rocks from an igneous province. The Wrangellia LIP, also called the
844 Nikolai LIP (Schmidt and Rogers, 2007; Greene *et al.*, 2010; Glen *et al.*, 2011), is indicated as the
845 most important contributor, possibly strengthened by other basaltic and acidic volcanic sources,
846 namely the South Taimyr igneous complex in Siberia plus the Kara Dere-Sayrun unit of the middle
847 Antalya nappes and the Huglu-Pindos volcanics in Turkey (Dal Corso *et al.*, 2012; Mueller *et al.*,
848 2016a; Sun *et al.*, 2016; Miller et al., 2017).

849 The remnants of the Wrangellia LIP today crop out along western North America, from
850 Vancouver Island (Canada) to Alaska (Greene *et al.*, 2010). The volcanic sequence consists of a
851 series of submarine pillow lavas and subaerial basaltic floods, locally reaching a thickness of 3.5
852 Km in Northern Wrangellia (Nikolai Fm., Alaska) and 6 Km in Southern Wrangellia (Karmutsen
853 Fm., Vancouver Island, Canada). It has been estimated that the Wrangellia LIP extruded at least 1
854 million Km^3 of basalts (Lassiter *et al.*, 1995). This figure is, however, a minimum estimate of the
855 volumes of basalts erupted because most of them could have been subducted as a consequence
856 of the accretion of the Wrangellia terranes to the western North America during the Late Jurassic–
857 Early Cretaceous (Greene *et al.*, 2010).

858 The age of the Wrangellia LIP is constrained by biostratigraphic data, $^{187}Os/^{188}Os$
859 geochemistry, and U-Pb, ^{40}Ar-^{39}Ar, and K-Ar radioisotopic ages (Mortensen and Hulbert, 1992;
860 Greene *et al.*, 2010; Glenn *et al.*, 2011; Xu *et al.*, 2014 and references therein). Limestones
861 intercalated and overlying the Wrangellia basalts bear a rich ammonoid association with *Tropites*
862 *dilleri*, which indicates a Tuvalian 1 age (Tozer, 1994). Silicified shales, locally black, chert and
863 limestones underlying the Wrangellia basalts contain *Daonella* bivalves, which indicate a Ladinian
864 age for these sediments (Greene *et al.*, 2010). A decrease in $^{187}Os/^{188}Os$ ratio is observed in the

865 Ladinian–Carnian prodelta–delta sediments of the Botneheia, Tschermakfjellet, and De Geerdalen
866 Formations of the Barents Sea (Norway), and has been interpreted as the evidence of a Ladinian
867 age for the beginning of Wrangellia LIP activity (Xu *et al.*, 2014). The $^{187}Os/^{188}Os$ excursion
868 consists, however, of only one data point, whose age is constrained to the late Ladinian by the
869 presence of *Nathorstites* sp. Juv., a boreal late Ladinian–early Carnian ammonoid genus (Xu *et al.*,
870 2014 and references therein). A higher resolution record in other settings coupled with a refined
871 biostratigraphy is thus required to confirm such a late Ladinian decrease in $^{187}Os/^{188}Os$ ratio. Most
872 of the ^{40}Ar-^{39}Ar ages of Wrangellia basalts are reset to ages younger than the age of the
873 emplacement of the LIP (Greene *et al.*, 2010; Glenn *et al.*, 2011 and references therein). Few of
874 the ^{40}Ar-^{39}Ar ages from biotites and horneblendes are considered to retain magmatic ages, which
875 span from 227 to 233 Ma (Greene *et al.*, 2010). The U-Pb data from multigrain zircon and
876 baddeleyite fractions give ages of 226.8±0.5 Ma, 227.3±2.6 Ma, 228.4±2.5 Ma, and 232.2±1 Ma,
877 which are though to reflect the magmatic age and are in agreement with a Carnian biostratigraphic
878 age of the Wrangellia LIP (Mortensen and Hulbert, 1992; Parrish and McNicoll, 1992; Greene *et*
879 *al.*, 2010). Summarizing, existing data constrain very well the end of Wrangellia LIP volcanism to
880 the Tuvalian 1 (*T. dilleri* ammonoid Zone). The onset of the LIP activity is, however, less well
881 constrained, although data suggest it could have been between the latest Ladinian and the early
882 Carnian.

883 Similar to the eruption of the Central Atlantic Magmatic Province at the end of the Triassic,
884 discrete pulses of Wrangellia activity could have caused multiple injections of ^{13}C-depleted CO_2
885 into the ocean–atmosphere system (e.g., Ruhl and Kürschner, 2011; Marzoli *et al.*, 2018). Such
886 CO_2 could have been released from methane clathrates ($\delta^{13}C$ = -60‰), as a consequence of
887 volcanically driven global warming, and/or from the metamorphism of organic-rich sediments ($\delta^{13}C$
888 = -25‰) in contact with igneous intrusions (e.g., Dickens *et al.*, 1995; Svensen *et al.*, 2004). Future
889 research should determine the timing of Wrangellia volcanic activity phases in detail, in order to
890 define possible distinct pulses, and test whether they correlate with the Carnian carbon-isotope
891 record.
892

6.5 Each carbon-isotope excursion is linked to environmental changes

The interval punctuated by the NCIEs within the Carnian, corresponding to the CPE, was a time of overall global warming as indicated by $\delta^{18}O$ analysis of conodont apatite (Fig. 9; Sun *et al.*, 2016 and references therein), and is closely related to environmental changes that are widespread at least across the Western Tethys (Fig. 9). Three to four distinct siliciclastic-dominated intervals are traditionally recognized in Carnian (Julian 2–Tuvalian 2) stratigraphic successions of the Western Tethys realm (e.g., see summary in Roghi *et al.*, 2010; Fig. 9). In the Dolomites, such terrigenous levels are located at the base of the Borca Mb., in the lower part of the Dibona Mb., and in the lower part of the Lagazuoi Mb. of the Heiligkreuz Formation. At the base of the Travenanzes Fm. a mixed carbonate–terrigenous level is also present (Fig. 2). These distinct levels can be recognized in other sections, and are biostratigraphically correlated within the Western Tethyan realm (Roghi *et al.*, 2010).

Roghi *et al.* (2010) and Stefani *et al.* (2010) interpreted the multiple siliciclastic levels as the stratigraphic evidence of discrete humid pulses. This interpretation is supported by palynological analyses of Western Tethyan successions that show distinct phases of hygrophytic-dominated assemblages in the siliciclastic intervals (Roghi *et al.*, 2010; Mueller *et al.*, 2016a; b). Evidence presented in this paper show that global NCIEs coincide with the siliciclastic-rich intervals. In fact, a likely consequence of large injections of isotopically depleted CO_2 into the atmosphere was, along with the NCIEs recorded by bulk organic matter, the enhancement of the hydrological cycle and associated continental runoff due to global warming. Under this climatic regime, large quantities of terrigenous material and nutrients would have flowed into marine basins, with development of local anoxic conditions and deposition of laminated organic-rich black shales (e.g., Jenkyns 2010). Such features are observed in several stratigraphic successions that register the NCIE 1 (Dal Corso *et al.*, 2015 and references therein). In summary, repeated episodes of enhanced terrigenous input and establishment of hygrophytic floras are here linked to phases of increased hydrological cycling, likely related to multiple phases of ^{13}C-depleted carbon injection into the Carnian ocean–atmosphere system over a time-span of 1.2 Myrs (Fig. 8, 9; Zhang *et al.*, 2015; Miller *et al.*, 2017).

The Carnian NCIEs also coincided with major changes in the carbonate production on shallow-water platforms. At the onset of the CPE in the Dolomites, a sudden shift of the carbonate production mode is observed from microbially induced carbonate precipitation to metazoan biomineralization, in coincidence with the NCIE-1 (Fig. 8; Dal Corso *et al.*, 2015; Gattolin *et al.*, 2015). Such a shift of the carbonate factory is noteworthy, because the highly productive microbial platforms had thrived in the shallow-water Tethyan domain and had persisted in the area of the Dolomites since the Anisian (e.g., Blendinger, 1994; Russo et al., 1997; Keim & Schlager, 1999; Preto *et al.*, 2017), and their temporary demise lasted throughout the entire CPE (Fig. 8; e.g., Gattolin *et al.*, 2015). Only during the Tuvalian 2 interval did the microbial carbonate factories return to dominance (e.g., Main Dolomite: Caggiati et al., in press). Outside the Dolomites, crises of shallow-water carbonate production are documented also for the South China Block (e.g., Sun *et al.*, 2016), the Southern Tethyan successions of the Spiti Valley in India (Hornung *et al.*, 2007) and Anatolia (Lukeneder *et al.*, 2012). In all of these localities, clays and sandstones abruptly substitute for the shallow-water carbonates. Contemporaneously, in the Lagonegro Basin in southern Italy, one of the very few basins that show a Carnian deep-water record, carbonate rocks were abruptly replaced by argillites, siltites, and radiolarites (clay-radiolaritic horizon) with no carbonate content at about the Julian–Tuvalian boundary, testifying to deep-water carbonate dissolution (Rigo *et al.*, 2007).

Dal Corso *et al.* (2012) argued that an injection of large quantities of CO_2 into the Carnian ocean–atmosphere system would have triggered an episode of acidification of the ocean, as suggested also for other similar events in the Earth's history. Ocean acidification could indeed explain the crisis of the microbial factories on platforms as well as the dissolution of deep-water carbonates. For example, deglacial ocean acidification has triggered an abrupt decline of calcified bacterial crusts in tropical reefs during the last 12 Kyrs (Riding *et al.*, 2014), and injection of CO_2 into the ocean resulted in the shoaling of the CCD and the dissolution of pelagic carbonates at the Palaeocene–Eocene thermal maximum (Zachos *et al.*, 2005). Modelling studies, however, indicate that ocean acidification cannot develop over time scales as long as those of the CPE (ca. 1.2 Myrs) (Ridgwell and Schmidt 2010; Hönisch *et al.*, 2012). Today's oceans would be relatively rapidly

buffered against acidification mainly by dissolution of vast amounts of pelagic carbonate sediments. In the Carnian, however, pelagic calcifiers were not so abundant and the buffering capacity of the oceans would have been much reduced, being limited to dissolution of shallow-water carbonates on platforms and surrounding peri-platform deposits (such as those of the Lagonegro Basin; Rigo et al., 2007), as well as the chemical weathering of carbonate and silicate rocks on land, as proposed also for the Late Permian (Payne et al., 2010). However, Zeebe *et al.* (2009), for example, suggested, for the Palaeocene–Eocene Thermal Maximum, a first rapid (5 Kyrs) injection of 3000 Gt of C followed by a second slower (ca. 50 Kyrs) injection of 1480 Gt of C into the atmosphere–ocean system. This timing could reproduce the duration of the carbonate dissolution event (70 Kyrs), reconstructed for Atlantic Ocean cores. Dal Corso *et al.* (2012) estimated that the Wrangellia LIP released a minimum of 5000 Gt of C, but, as previously explained, additional inputs of ^{13}C-depleted C from ocean-floor clathrates and/or from organic-rich sediments must be hypothesized to explain the NCIEs, given the fact that LIPs are thought to release C that is isotopically heavier than these other sources ($\delta^{13}C$ = ca. -6‰; Dickens *et al.*, 1995). Therefore, we suggest that the release in pulses of a huge amount of C (volcanic plus clathrate and/or organic) into the Carnian ocean–atmosphere system, coupled with much slower ocean buffering, could have sustained prolonged episodes of ocean acidification. Pulsed release of CO_2 could have similarly caused the protracted global warming recorded by conodont apatite (Fig. 9). The deep-water clay-radiolaritic horizon of the Lagonegro Basin (Rigo *et al.*, 2007), deposited at a lower sedimentation rate than all other successions considered in this study, may lump together all sub-events in an apparently unique environmental perturbation, which lasted throughout the CPE.

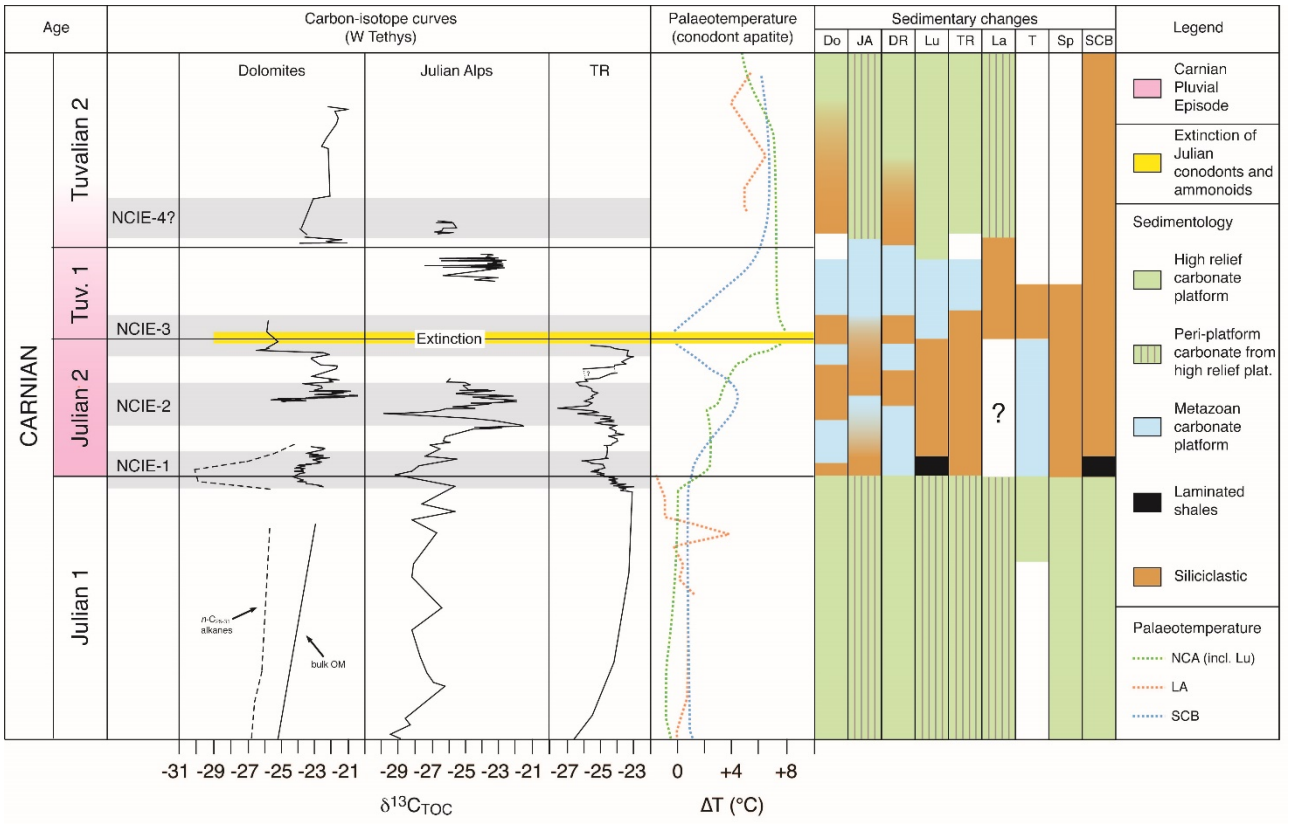

Figure 9. Organic carbon-isotope curves for the Julian 1–Tuvalian 2 interval of the Carnian Stage. Three, possibly four, carbon-isotope excursions in the exchangeable reservoirs of the global carbon cycle punctuated the Carnian Pluvial Episode. These excursions are linked to discrete humid pulses as indicated by the sedimentary record of different siliciclastic inputs in many different geological settings. This interval of multiple carbon-cycle perturbations corresponds to an interval of overall global warming and sudden changes in carbonate production on shallow-water platforms. The third negative excursion is linked to the extinction of the *Trachyceratinae* ammonoids and 70% of conodont genera, approx. 1.2 Myrs after the onset of the Carnian Pluvial Episode and the first carbon-cycle perturbation. Ages are from Zhang *et al.* (2016). The palaeotemperatures calculated from oxygen-isotope analysis of conodont apatite are from Hornung *et al.,* (2007), Rigo and Joachimski (2010), Trotter *et al.* (2015), and Sun *et al.*, (2016). Abbreviations and selected references: Do = Dolomites (Preto and Hinnov, 2003); JA = Julian Alps (De Zanche *et al.*, 2000 and this study); DR = Drau Range (Roghi et al., 2010); Lu = Lunz (Roghi et al., 2010); TR = Transdanubian Range (Budai and Haas, 1997); T = Turkey (Lukeneder *et al.*, 2012); La = Lagonegro (e.g. Rigo *et al.*, 2007); Sp = Spiti (Hornung *et al.*, 2007); SCB = South China Block (Sun *et al.*, 2016).

6.6 Multiple carbon-isotope excursions and stepwise biotic turnover

The carbon-cycle perturbations during the CPE coincided also with an interval of major biotic turnover (Benton 1986). Many marine taxa became extinct during the CPE, including crinoids, echinoids, bivalves, bryozoan, conodonts, and ammonoids (Simms and Ruffell, 1989; Hallam 1995). For example, the *Encrinidae*, the most distinctive group of crinoids in the Triassic, as well as other important groups like the *Isocrinina*, completely disappeared or severely declined during the CPE (Simms and Ruffell, 1990). In general, analysis of functional diversity across the entire Late Triassic indicated that benthic suspension feeding suffered a great loss during the CPE, probably because of increasing sediment input and eutrophication in shallow-water environments (Dunhill *et al.*, 2017). The exact timing of these extinctions with respect to NCIEs is, however, unknown, whereas the timing of extinction of biostratigraphically significant pelagic groups is much better constrained. Approximately 70% of conodont genera became extinct at the Julian–Tuvalian boundary (Rigo et al., 2007; Martínez-Pérez *et al.*, 2015; Chen *et al.*, 2015). Contemporaneously, the dominant ammonoid group, the *Trachyceratinae*, virtually disappeared and was substituted by the *Tropitidae* (e.g., Tozer, 1967; Krystyn 1991; Balini *et al.*, 2010). Therefore, the extinction of conodonts and ammonoids can be stratigraphically correlated to the NCIE-3 (Fig. 6). This extinction in pelagic marine environments seems to have been slightly preceded by the appearance of the first abundant pelagic calcifiers (calcareous nannofossils or calcispheres, possibly related to calcareous dinocysts) in late Julian and Tuvalian marine successions of the north western Tethys (e.g., Jafar, 1983; Janofske, 1992; Bellanca et al, 1995; Preto *et al.*, 2013).

On land, a major turnover in the flora and vertebrate fauna is documented for the Carnian, although the timing of this event is more difficult to constrain precisely with biostratigraphy. Palynological studies show a peak of diversity during the Julian 2 (early Carnian) and sporomorph assemblages are dominated by hygrophytic elements, probably an indication of more humid climatic conditions (e.g., Roghi 2004; Kürschner and Herngreen, 2010). Subsequently, a huge decline (ca. 50%) in sporomorph diversity between the early Carnian and the Norian is documented, which is the second most severe decline of microfloras after the Permian–Triassic boundary mass extinction (Kürschner and Herngreen, 2010). Meanwhile, the circumpolles

(*Cheirolepidiaceae*) group underwent a major diversification (Kürschner and Herngreen, 2010). The radiation of modern conifers and benettitaleans also occurred during the Carnian (Wills and McElwain., 2002; Kustatscher et al., 2018). Severe extinction in the Late Carnian is known among the tetrapod fauna: rhynchosaurs, dicynodonts, and chiniquodontids were essentially extinct by the end of the Carnian (Benton, 1986; Benton, 1991; Brusatte *et al.*, 2008; Lucas and Tanner, 2015). The first major diversification of the dinosaurs in the Tuvalian was close in time with, and maybe favoured by, the extinction of the tetrapod fauna (Brusatte *et al.*, 2008), and the earliest mammals also date back to the Tuvalian (Lucas and Luo, 1993; Kemp, 2005; Datta, 2005; Newham *et al.*, 2014). Notably, comparison of diversity patterns shows that terrestrial turnover of the Carnian was much more important than that at the Triassic–Jurassic boundary, where there is no strong signal of extinction/radiation among vertebrate fauna and flora (e.g., Benton, 1986; Lucas and Tanner, 2015; Kürschner and Herngreen, 2010; Barbacka *et al.*, 2017 and references therein).

7. CONCLUSIONS

A review of the existing carbon-isotope records and new carbon-isotope analysis of organic matter, coupled to a refined biostratigraphic calibration of marine sedimentary successions of the Tethyan realm (Dolomites and Julian Alps in Italy, and Transdanubian Range in Hungary) shows that three, possibly four, major negative shifts punctuated the Carnian Pluvial Episode. The first negative $\delta^{13}C_{TOC}$ shift, already recognized in many different geological settings, occurred at the time of the Julian 1–Julian 2 boundary. The second is placed within the Julian 2; the third negative $\delta^{13}C_{TOC}$ shift happened at the Julian–Tuvalian boundary; and a possible fourth excursion is recorded in the Dolomites at the Tuvalian 1–Tuvalian 2 boundary. The occurrence of the first three shifts in different sedimentary archives at the same stratigraphic levels, Rock-Eval pyrolysis analysis, and wood carbon-isotope data show that the $\delta^{13}C$ excursions represent genuine changes in the isotopic composition of the exchangeable reservoirs of the carbon cycle. The timing of the negative $\delta^{13}C$ shifts is such that they coincided with discrete humid pulses, which can explain the enhanced siliciclastic input into the basins and the crisis of shallow-water carbonate depositional systems observed worldwide. Moreover, the results of our study envisage a potential link between

extinctions and radiations near the Julian–Tuvalian boundary, and the third negative carbon-isotope excursion of the Carnian Pluvial Episode. New and literature data show that repeated injections of ^{13}C-depleted CO_2 into the Carnian ocean-atmosphere system triggered distinct climatic perturbations, which resulted in the disruption of environments and ecosystems. Similarly to other LIP-related climatic shifts in Earth's history, different eruptive pulses of the Wrangellia (Nikolai) LIP triggered the carbon-cycle perturbations and led to extinctions at the Julian–Tuvalian boundary.

ACKNOWLEDGMENTS

We thank P. Scotti (ENI) for the Rock-Eval analysis and useful suggestions, and P. Ditchfield for isotope analyses at the Research Laboratory for Archaeology and the History of Art (Oxford, UK). C. Agnini contributed to the fine-tuning of IRMS methods at the University of Padova (Italy). We thank the editor A. Strasser, Y. Sun and two anonymous reviewers for their comments that greatly improved the manuscript.

FUNDING

J. Dal Corso was funded by Young Researcher Grant of the University of Padova (Italy) (Acronym: DALCPRGR12), and by a Junior Fellowship of the Hanse-Wissenschaftskolleg (HWK), Institute for Advanced Study in Delmenhorst (Germany) (cooperation partner: A. Merico, ZMT Bremen). P. Gianolla and M. Caggiati were funded by the Italian Government PRIN 2010-2011 funds (Pr. No. 20107ESMX9_004). N. Preto was funded by the University of Padova (grant CPDA121100), and by the Alexander von Humboldt Foundation.

DECLARATIONS OF INTEREST

None

REFERENCES

1) Arche, A., López-Gómez, J.L., 2014. The Carnian Pluvial Event in Western Europe: new data from Iberia and correlation with the Western Neotethys and Eastern North America–NW Africa regions. Earth-Sci. Rev. 128, 196–231. doi.org/10.1016/j.earscirev.2013.10.012

2) Arthur, M.A., Dean, W.E., Claypool, G.E., 1985. Anomalous ^{13}C enrichment in modern marine organic carbon. Nature 315, 216–218.

3) Balini, M., Lucas, S.G., Jenks, J.F., Spielmann, J.A., 2010. Triassic ammonoid biostratigraphy: an overview. Geol. Soc. (Lond.) Spec. Publ. 334, 221–262. doi.org/10.1144/SP334.10

4) Benton, M.J., 1986. More than one event in the Late Triassic mass extinction. Nature 321, 857–861. doi:10.1038/321857a0

5) Benton, M.J., 1991. What really happened in the late Triassic? Historical Biology 5, 263–278. doi.org/10.1080/10292389109380406

6) Bernardi, M., Gianolla, P., Petti, F.M., Mietto, P., Benton, M.J., 2018. Dinosaur diversification linked to the Carnian Pluvial Episode. Nat. Comm. 9, 1499. doi:10.1038/s41467-018-03996-1

7) Bizzarini, F., 2000. Studio biostratigrafico delle tanatocenosi a cefalopodi della Formazione di S. Cassiano (Valle d'Ampezzo, Dolomiti orientali). Lavori Soc. Ven. Sc. Nat. 25, 15–28.

8) Bizzarini, F., Braga, G., 1987: Considerazioni bio e litostratigrafiche sulla Formazione di S. Cassiano (Dolomiti Nord-Orientali, Italia). - Studi Trentini di Scienze Naturali, 64, pp. 39-56.

9) Blendinger, W., 1994. The carbonate factory of Middle Triassic buildups in the Dolomites, Italy: a quantitative analysis. Sedimentology 41, 1147–1159. doi.org/10.1111/j.1365-3091.1994.tb01446.x

10) Breda, A., Preto, N., Roghi, G., Furin, S., Meneguolo, R., Ragazzi, E., Fedele, P., Gianolla, P., 2009. The Carnian Pluvial Event in the Tofane area (Cortina d'Ampezzo, Dolomites, Italy). Geol.Alp 6, 80–115.

11) Breda, A., Preto, N., 2011. Anatomy of an Upper Triassic continental to marginal-marine system: The mixed siliciclastic-carbonate Travenanzes Formation (Dolomites, Northern Italy). Sedimentology 58, 1613–1647.Brusatte, S.L., Benton, M.J., Ruta, M., Lloyd, G.T., 2008. Superiority, competition, and opportunism in the evolutionary radiation of the dinosaurs. Science 321, 1485–1488. doi.org/10.1111/j.1365-3091.2011.01227.x

12) Budai, T., Haas, J., 1997. Triassic sequence stratigraphy of the Balaton Highland, Hungary. Acta Geol. Hung. 40/3, 307–335.

13) Budai, T., Csaszar, G., Csillag, G., Dudko, A., Koloszar, L., Majaros, G., 1999. Geology of the Balaton Highland. Occasional Papers, Geological Institute of Hungary, Budapest, p. 197.

14) Caggiati, M., Gianolla, P., Breda, A., Celarc, B., Preto N., 2017. The start-up of the Dolomia Principale/Hauptdolomit carbonate platform (Upper Triassic) in the eastern Southern Alps. Sedimentology. doi: 10.1111/sed.12416. doi.org/10.1111/sed.12416

15) Chen, Y, Krystyn, L., Orchard, M.J., Lai, X.-L., Richoz, S., 2015. A review of the evolution, biostratigraphy, provincialism and diversity of Middle and early Late Triassic conodonts. Pap. Palaeontol., 2, 235–263. doi.org/10.1002/spp2.1038

16) Dal Corso, J., Preto, N., Kustatscher, E., Mietto, P., Roghi, G., Jenkyns, H.C, 2011. Carbon-isotope variability of Triassic amber, as compared with wood and leaves (Southern Alps, Italy). Palaeogeogr. Palaeoclimatol. Palaeoecol. 302, 187– 193. doi.org/10.1016/j.palaeo.2011.01.007

17) Dal Corso, J., Mietto, P., Newton, R.J., Pancost, R.D., Preto, N., Roghi, G., Wignall, P.B., 2012. Discovery of a major negative $\delta^{13}C$ spike in the Carnian (Late Triassic) linked to the eruption of Wrangellia flood basalts. Geology 40, 79–82. doi.org/10.1130/G32473.1

18) Dal Corso, J., Gianolla, P., Newton, R.J., Franceschi, M., Roghi, G., Caggiati, M., Raucsik, B., Budai, T., Haas, J., Preto, N., 2015. Carbon isotope records reveal synchronicity between

carbon cycle perturbation and the “Carnian Pluvial Event” in the Tethys realm (Late Triassic). Glob. Planet. Change 127, 79–90. doi.org/10.1016/j.gloplacha.2015.01.013

19) Dal Corso, J., Schmidt, A.R., Seyfullah, L. J., Preto,N., Ragazzi, E., Jenkyns, H. C., Delclos, X., Neraudeau, D., Roghi, G., 2017. Evaluating the use of amber in palaeoatmospheric reconstructions: the carbon-isotope variability of modern and Cretaceous conifer resins. Geochim. Cosmochim. Acta 199, 351–369. doi.org/10.1016/j.gca.2016.11.025

20) Dal Corso, J., Benton, M.J., Bernardi, M., Franz, M., Gianolla, P., Hohn, S., Kustatscher, E., Merico, A., Roghi, G., Ruffell, A., Ogg, J.G., Preto, N., Schmidt, A.R., Seyfullah, L.J., Simms, M.J., Shi, Z., Zhang, Y., 2018. First workshop on the Carnian Pluvial Episode (Late Triassic): A report. Albertiana 44, 49–57.

21) Datta, P.M., 2005. Earliest mammal with transversely expanded upper molar from the Late Triassic (Carnian) Tiki Formation, South Rewa Gondwana Basin, India. J. Vert. Paleontol., 25, 200–207. doi.org/10.1671/0272-4634(2005)025[0200:EMWTEU]2.0.CO;2

22) De Zanche, V., Gianolla, P., Roghi, G., 2000. Carnian stratigraphy in the Raibl/Cave del Predil area (Julian Alps, Italy). Eclogae Geol. Helv. 93, 331–347.

23) Dickens, G.D., O’Neil, J., Rea, D.K., Owen, R.M. 1995. Dissociation of methane hydrate as a cause of the carbon isotope excursion at the end of the Paleocene. Paleoceanography, 10, 965–971.

24) Diefendorf, A. F., Mueller, K. E., Wing, S. L., Koch, P. L., Freeman, K. H., 2010. Global patterns in leaf ^{13}C discrimination and implications for the studies of past and future climate. Proc. Nat. Acad. Sci. 107, 5738–5743. doi.org/10.1073/pnas.0910513107

25) Dosztály, L., S. Kovács, T. Budai, 1989. Pécsely, Meggy hegy quarry. In XXI Europea Micropalaeontological Colloquium, Guidebook.

26) Dunhill, A.M., Foster, W.J., Sciberras, J., Twitchett, R.J., 2017. Impact of the Late Triassic mass extinction on functional diversity and composition of marine ecosystems. Palaeontology, doi.org/10.1111/pala.12332

27) Franz, M., Nowak, K., Berner, U., Haunisch, C., Bandel, K., Rohling, H.G., Wolfgramm, M., 2014. Eustatic control on epicontinental basins: the example of the Stuttgart Formation in the Central European Basin (Middle Keuper, Late Triassic). Glob. Planet. Change 122, 305–329. doi.org/10.1016/j.gloplacha.2014.07.010

28) Furin, S., Preto, N., Rigo, M., Roghi, G., Giannola, P., Crowley, J.L., Bowring, S.A., 2006. High-precision U–Pb zircon age from the Triassic of Italy: implications for the Triassic time scale and the Carnian origin of calcareous nannoplankton and dinosaurs. Geology 34, 1009–1012. doi.org/10.1130/G22967A.1

29) Galimov, E.M., 2006. Isotope organic geochemistry. Org. Geochem. 37, 1200–1262. http://dx.doi.org/10.1016/j.orggeochem.2006.04.009.

30) Gattolin, G., Preto, N., Breda, A., Franceschi, M., Isotton, M., Gianolla, P., 2015. Sequence stratigraphy after the demise of a high-relief carbonate platform (Carnian of the Dolomites): Sea-level and climate disentangled. Palaeogeogr. Palaeoclimatol. Palaeoecol. 423, 1–17. doi:10.1016/j.palaeo.2015.01.017

31) Gianolla, P., De Zanche, V., Mietto, P. 1998. Triassic sequence stratigraphy in the Southern Alps (northern Italy): definition of sequences and basin evolution. In: De Graciansky, P.C., Hardenbol, J., Jacquin, T., Vail, P.R. (Eds.), Mesozoic and Cenozoic Sequence Stratigraphy of European Basins. SEPM Special Publication 60, 719–748.

32) Gianolla, P., De Zanche, V., and Roghi, G., 2003. An Upper Tuvalian (Triassic) Platform-Basin System in the Julian Alps: the Start-up of the Dolomia Principale (Southern Alps, Italy). Facies, 49, 135–150. doi.org/10.1007/s10347-003-0029-7

1173 33) Glen, J.M.G., Schmidt, J.M., Connard, G.G., 2011. Three-dimensional model of an ultramafic
1174 feeder system to the Nikolai Greenstone mafic large igneous province, central Alaska Range.
1175 Geochem. Geophys. Geosyst. 12, Q06018. doi.org/10.1029/2011GC003508

1176 34) Góczán, F., Oravecz–Scheffer, A., 1996a. Tuvalian sequences of the Balaton Highland and
1177 the Zsámbék Basin, Part I: Litho-, bio- and chronostratigraphic subdivision. Acta Geol. Hung.
1178 39/1, 1–31.

1179 35) Góczán, F., Oravecz–Scheffer, A., 1996b. Tuvalian sequences of the Balaton Highland and
1180 the Zsámbék Basin, Part II: Characterization of sporomorph and foraminifer assemblages,
1181 biostratigraphic, palaeogeographic and geohistoric conclusions. Acta Geol. Hung. 39/1, 33–
1182 101.

1183 36) Góczán, F., A. Oravecz-Scheffer, G. Csillag, 1991. The stratigraphic characterization of the
1184 Cordevolian and Julian Formations of Csukréti Ravine, Balatoncsicsó. Földt. Int. Évi Jel.
1185 1989-ról, 241–323.

1186 37) Greene, A.R., Scoates, J.S., Weis, D., Katvala, E.C., Israel, S., Nixon, G.T., 2010. The
1187 architecture of oceanic plateaus revealed by the volcanic stratigraphy of the accreted
1188 Wrangellia oceanic plateau. Geosphere 6, 47–73. doi.org/10.1130/GES00212.1

1189 38) Gröcke, D.R., Hesselbo, S.P., Jenkyns, H.C., 1999. Carbon-isotope composition of Lower
1190 Cretaceous fossil wood: Ocean–atmosphere chemistry and relation to sea-level change.
1191 Geology, 27, 155–158. doi.org/10.1130/0091-7613(1999)027<0155:CICOLC>2.3.CO;2

1192 39) Haas, J., Budai, T., 1999. Triassic sequence stratigraphy of the Transdanubian Central
1193 Range (Hungary). Geol. Carpath. 50/6, 459–475.

1194 40) Haas, J., Budai, T., 2004. Dunántúli-középhegységi egység. In: Haas, J. (Ed.),
1195 Magyarország geológiája, Triász. ELTE Eötvös Kiadó, Budapest, pp. 25–124.

41) Hallam, T., 1995. Major Bio-Events in the Triassic and Kurassic. In: Walliser, O.H., Global Events and Event Stratigraphy, Springer-Verlag Berlin Heidelberg New York, pp. 265–283.

42) Hesselbo, S. P., Jenkyns, H. C., Duarte, L. V., Oliveira, L. C., 2007. Carbon-isotope record of the Early Jurassic (Toarcian) Oceanic Anoxic Event from fossil wood and marine carbonate (Lusitanian Basin, Portugal). Earth Planet. Sci. Lett. 253, 455– 470. doi.org/10.1016/j.epsl.2006.11.009

43) Hönisch, B., Ridgwell, A., Schmidt, D.N., Thomas, E., Gibbs, S.J., Sluijs, A., Zeebe, R., Kump, L., Martindale, R.C., Greene, S.E., Kiessling, W., Ries, J., Zachos, J.C., Royer, D.L., Barker, S., Marchitto, T.M.Jr, Moyer, R., Pelejero, C., Ziveri, P., Foster, G.L., Williams, B., 2012. The geological record of ocean acidification. Science 335, 1058–1063. DOI: 10.1126/science.1208277

44) Hornung, T., Brandner, R., 2005. Biochronostratigraphy of the Reingraben Turnover (Hallstatt Facies Belt): local black shale events controlled by regional tectonics, climatic change and plate tectonics. Facies 51, 460–479. doi.org/10.1007/s10347-005-0061-x

45) Hornung, T., Krystyn, L., Brandner, R., 2007. A Tethys-wide mid-Carnian (Upper Triassic) carbonate productivity crisis: Evidence for the Alpine Reingraben Event from Spiti (Indian Himalaya)? J. Asian Earth Sci. 30, 285–302. doi.org/10.1016/j.jseaes.2006.10.001

46) Janofske, D., 1992. Kalkiges nannoplankton, insbesondere kalkige Dinoflagellate-Zysten der Alpine Ober-Trias: Taxonomie, Biostratigraphie und Bedeuntung fur die Phylogenie der Peridinales. Berliner Geowissenschaften Abh. E 4, 1–93.

47) Jenkyns, H.C., 2010. Geochemistry of oceanic anoxic events. Geochem. Geophys. Geosyst.,11(3), Q03004. doi.org/10.1029/2009GC002788

48) Jenks, J.F., Monnet, C., Balini, M., Brayard, A., Meier, M., Biostratigraphy of Triassic ammonoids. In C. Klug et al. (eds.), Ammonoid Paleobiology: From macroevolution to paleogeography. Topics in Geobiology 44.

49) Keim, L., Schlager, W., 2001. Quantitative compositional analysis of a Triassic carbonate platform (Southern Alps, Italy). Sediment. Geol. 139, 261–283. doi.org/10.1016/S0037-0738(00)00163-9

50) Keim, L., Spötl, C., Brandner, R., 2006. The aftermath of the Carnian carbonate platform demise: a basinal perspective (Dolomites, Southern Alps). Sedimentology 53, 361–386. doi.org/10.1111/j.1365-3091.2006.00768.x

51) Kemp, TS., 2005 The origin and evolution of mammals. Oxford, UK: Oxford University Press. 331 p.

52) Kohn, M. J., 2016. Carbon isotope discrimination in C3 land plants is independent of natural variations in pCO_2. Geochem. Perspect. Lett. 2, 35–43. doi: 10.7185/geochemlet.1604

53) Kolar-Jurkovšek, T., Gaździcki, A., Jurkovšek, B., 2005. Conodonts and foraminifera from the "Raibl Beds" (Carnian) of the Kararvanke Mountains, Slovenia: stratigraphical and paleontological implications. Geol. Quart. 49/4, 429–438.

54) Kolar-Jurkovšek, T., Jurkovšek, B., 2010. New paleontological evidence of the Carnian strata in the Mežica area (Karavanke Mountains, Slovenia): conodont data for the Carnian Pluvial Event. Palaeogeogr. Palaeoclimatol. Palaeoecol. 290, 81–8. DOI: 10.1016/j.palaeo.2009.06.015

55) Korte, C., Kozur, H., Veizer, J., 2005. $\delta^{13}C$ and $\delta^{18}O$ values of Triassic brachiopods and carbonate rocks as proxies for coeval seawater and palaeotemperature. Palaeogeogr. Palaeoclimatol. Palaeoecol. 226, 287–306. doi.org/10.1016/j.palaeo.2005.05.018

56) Kozur, H., Mock, R., 1991. New Middle Carnian and Rhaetian Conodonts from Hungary and the Alps. Stratigraphic importance and tectonic implications for the Buda Mountains and adjacent areas. Jb. Geol. B.-A. 134/2, 271–297.

57) Kovács, S., L. Krystyn, S. Szabó, L. Dosztály, and T. Budai, 1991. The Ladinian/Carnian boundary in the Balaton Upland, Hungary. Symp. Trias. Strat.

58) Kristan-Tollmann, E., Haas, J., Kovács, S., 1991. Karnische Ostracoden und Conodonten der Bohrung Zsámbék–14 im Transdanubischen Mittelgebirge (Ungarn). Jubiläumsschrift 20 Jahre Geologische Zusammenarbeit Österreich–Ungarn, 193–220.

59) Krystyn, L., 1991. Die Fossillagerstätten der alpinen Trias: Exkursionsführer. Universität Wien, p. 61.

60) Krystyn, L., 1978. Eine neue Zonengliederung im alpin-mediterranen Unterkarn. Schrift. Erdwiss. Komm. Österr. Ak. Wiss., v. 4, pp. 37-75, Wien.

61) Kürschner, W.M., Herngreen,W., 2010. Triassic palynology of central and northwestern Europe: a review of palynofloral diversity patterns and biostratigraphic subdivisions In: Lucas, S.G. (Ed.) The Triassic Timescale. Geol. Soc. Spec. Publ. 334, 263–283.

62) Kustatscher, E., Ash, S.R., Karasev, E., Pott, C., Vajda, V., Yu, J. & McLoughlin, S. 2018. Flora of the Late Triassic. In: Tanner, L. (ed.) The Late Triassic World: Earth in a Time of Transition. Topics in Geobiology, 46: 545-622, Springer, ISBN 978-3-319-68008-8.

63) Lassiter, J.C., DePaolo, D.J., Mahoney, J.J., 1995. Geochemistry of the Wrangellia flood basalt province: implications for the role of continental and oceanic lithosphere in flood basalt genesis. J. Petrol. 36, 983–1009. DOI: 10.1093/petrology/36.4.983

64) Leonardi P., Polo, C., 1952. La fauna cassiana di Cortina d'Ampezzo. Parte 2., Cefalopodi. Memorie dell'Istituto Geologico dell'Università di Padova, 17, 3–27.

65) Lewan, M.D., 1983. Effects of thermal maturation on stable organic carbon isotopes as determined by hydrous pyrolysis of Woodford Shale. Geochim. Cosmochim. Acta 47, 1471–1479. doi.org/10.1016/0016-7037(83)90306-X

66) Lieberman, H. M., 1978. Carnitza Formation — ein neuer Begriff für Oberkarnische Beckenkalke der südlichen Kalkalpen bei Raibl (Cave del Predil, Italien). Mitt. Ges. Geol. Bergbaustud. Österr., 25, 35–60.

67) Lucas, S.G., Luo, Z., 1993. Adebasileus from the Upper Triassic of West Texas: The Oldest Mammal. J. Vert. Paleontol. 13, 309–334.

68) Lucas, S.G., Tanner, L.H., 2015. End-Triassic nonmarine biotic events. Journal of Palaeogeography 4, 331–348. doi.org/10.1016/j.jop.2015.08.010

69) Lukeneder S., Lukeneder A., Harzhauser M., Islamoglu Y., Krystyn L., Lein R., 2012. A delayed carbonate factory breakdown during the Tethyan-wide Carnian Pluvial Episode along the Cimmerian terranes (Taurus, Turkey). Facies, 58, 279–296. doi.org/10.1007/s10347-011-0279-8

70) Lukeneder, S., Lukeneder, A., 2014. A new ammonoid fauna from the Carnian (Upper Triassic) Kasimlar Formation of the Taurus Mountains (Anatolia, Turkey). Palaeontology 57, 357–396. doi.org/10.1111/pala.12070

71) Maron, M., Muttoni, G., Dekkers, M.J., Mazza, M., Breda, A., Krijgsman, W., Rigo, M., 2017. Contribution to the magnetostratigraphy of the Carnian: new magneto-biostratigraphic constraints from Pignola-2 and Dibona marine sections, Italy. Newsl. Stratigr. 50, 187–203. DOI: 10.1127/nos/2017/0291

72) Martinez-Peréz, C., Cascales-Minana, B., Plasencia, P., Botella, H., 2014. Exploring the major depletions of conodont diversity during the Triassic. Hist. Biol. 27, 503–507. doi.org/10.1080/08912963.2014.890192

73) Marzoli, A., Callegaro, S., Dal Corso, J., Davies, J.H.F.L., Chiaradia, M., Youbi, N., Bertrand, H., Reisberg, L., Merle, R., Jourdan, F., 2018. The Central Atlantic Magmatic Province: a review. In: Tanner, L. (ed.) The Late Triassic World: Earth in a Time of Transition. Topics in Geobiology, 46: 545-622, Springer, ISBN 978-3-319-68008-8.

1292 74) Mastandrea, A. 1994. Carnian conodonts from Upper Triassic strata of Tamarin section (San
1293 Cassiano Fm., Dolomites, Italy). Riv. It. Paleont. Strat., 100, 493–510.

1294 75) Mazza, M., Rigo, M., Nicora, A., (2011). A new *Metapolygnathus* platform conodont species
1295 and its implications for Upper Carnian global correlations. Acta Palaeontol. Pol., 56, 121–
1296 131. dx.doi.org/10.4202/app.2009.1104

1297 76) Mazza, M., Rigo, M., Gullo, M. 2012a. Taxonomy and stratigraphic record of the Upper
1298 Triassic conodonts of the Pizzo Mondello section (Western Sicily, Italy), GSSP candidate for
1299 the base of the Norian. Riv. Ital. Paleontol. S., 118, 85–130. doi.org/10.13130/2039-
1300 4942/5993

1301 77) Mazza, M., Cau, A., and Rigo, M. 2012b. Application of numerical cladistic analyses to the
1302 Carnian-Norian conodonts: a new approach for phylogenetic interpretations. J. Syst.
1303 Palaeontol. 10, 401–422. doi.org/10.1080/14772019.2011.573584

1304 78) McKirdy, D.M., Powell, T.G., 1974. Metamorphic alteration of carbon isotopic composition in
1305 ancient sedimentary organic matter: new evidence from Australia and South Africa. Geology,
1306 2, 591–595. doi.org/10.1130/0091-7613(1974)2<591:MAOCIC>2.0.CO;2

1307 79) Mietto P., Manfrin S., Preto N., Rigo M., Roghi G., Furin S., Gianolla P., Posenato R.,
1308 Muttonii G., Nicora A., Buratti N., Cirilli S., Spötl C., Ramezani J., Bowring S.A., 2012. The
1309 Global Boundary Stratotype Section and Point (GSSP) of the Carnian Stage (Late Triassic)
1310 at Prati di Stuores/Stuores Wiesen section (Southern Alps, NE Italy). Episodes 35/3, 414–
1311 430. 10.18814/epiiugs/2012/v35i3/59614

1312 80) Miller, C.S., Peterse, F., da Silva, A.-C., Baranyi, V., Reichart, G.J., Kürschner, W., 2017.
1313 Astronomical age constraints and extinction mechanisms of the Late Triassic Carnian crisis.
1314 Sci. Rep. 2557. doi:10.1038/s41598-017-02817-7

1315 81) Mojsisovics, E.M. von, 1882. Die Cephalopoden der mediterranen Triasprovinz. Abh. K. K.
1316 Geol. Reichsanst. 10, 1–332, Wien.

82) Mortensen, J.K., Hulbert, L.J., 1992. A U-Pb zircon age for a Maple Creek gabbro sill, Tatamagouche Creek area, southwestern Yukon Territory, *in* Radiogenic age and isotopic studies: Report 5: Geological Survey of Canada Paper 91-2, p. 175–179 p.

83) Mueller, S., Krystyn, L., Kürschner, W.M., 2016a. Climate variability during the Carnian Pluvial Phase – a quantitative palynological study of the Carnian sedimentary succession at Lunz am See, Northern Calcareous Alps, Austria. Palaeogeogr. Palaeoclimatol. Palaeoecol. 441, 198–211. doi.org/10.1016/j.palaeo.2015.06.008

84) Mueller, S., Hounslow, M.W., Kürschner, W.M., 2016b. Integrated stratigraphy and palaeoclimate history of the Carnian Pluvial Event in the Boreal realm; new data from the Upper Triassic Kapp Toscana Group in central Spitsbergen (Norway). J. Geol. Soc. 173, 186–202. doi.org/10.1144/jgs2015-028

85) Muttoni, G., Mazza, M., Mosher, D., Katz, M.E., Kent, D.V., Balini, M., 2014. A Middle–Late Triassic (Ladinian–Rhaetian) Carbon and Oxygen isotope record from the Tethyan Ocean. Palaeogeogr. Palaeoclimatol. Palaeoecol. 399, 246–259. doi.org/10.1016/j.palaeo.2014.01.018

86) Neri, C., P. Gianolla, S. Furlanis, R. Caputo and A. Bosellini, 2007. Note Illustrative della Carta Geologica d'Italia alla scala 1:50.000, Foglio 029 Cortina d'Ampezzo. SystemCart, 200 p., Roma, A.P.A.T.

87) Newham, E., Benson, R., Upchurch, P., Goswami, A., 2014. Mesozoic mammaliaform diversity: The effect of sampling corrections on reconstructions of evolutionary dinamics. Palaeogeogr. Palaeoclimatol. Palaeoecol. 412, 32–44. doi.org/10.1016/j.palaeo.2014.07.017

88) Orchard, M.J., 2014. Conodonts from the Carnian-Norian Boundary (Upper Triassic) of Black Bear Ridge, Northeastern British Columbia, Canada. New Mexico Museum of Natural History and Science Bullettin, 64. 139 pp. New Mexico Museum of Natural History and Science, Albuquerque.

89) Payne, J.L., Turchyn, A.V., Paytan, A., DePaolo, D.J., Lehrmann, D.J., Yu, M., Wei, J., 2010. Calcium isotope constrains on the end-Permian mass extinction. Proc. Natl. Acad. Sci. 107, 8543–8548. doi.org/10.1073/pnas.0914065107

90) Preto, N., 2012. Petrology of carbonate beds from the stratotype of the Carnian (Stuores Wiesen section, Dolomites, Italy): the contribution of platform-derived microbialites. Geo.Alp 9, 12–29.

91) Preto, N., Hinnov, L., 2003. Unrevealing the origin of carbonate platform cyclothems in the Upper Triassic Durrenstein Formation (Dolomites, Italy). J. Sediment. Res. 73, 774–789. doi.org/10.1306/030503730774

92) Preto, N., Roghi, G., Gianolla, P., 2005. Carnian stratigraphy of the Dogna area (Julian Alps, northern Italy): tesserae of a complex palaeogeography. Bull. Soc. Geol. It. 124, 269–279.

93) Preto, N., Kustatscher, E., Wignall, P.B., 2010. Triassic climates—state of the art and perspectives. Palaeogeogr. Palaeoclimatol. Palaeoecol. 290, 1–10. doi.org/10.1016/j.palaeo.2010.03.015

94) Preto, N., Breda, A., Dal Corso, J., Spötl, C., Zorzi, F., Frisia, S., 2015. Primary dolomite in the Late Triassic Travenanzes Formation, Dolomites, Northern Italy: Facies control and possible bacterial influence. Sedimentology 62, 697–716. **doi.org/10.1111/sed.12157**

95) Preto, N., Gianolla, P., Franceschi, M., Gattolin, G., Riva, A., 2017. Geometry and evolution of Triassic high-relief, isolated microbial platforms in the Dolomites, Italy: The Anisian Latemar and Carnian Sella platforms compared. AAPG Bull. 101, 475–483. doi.org/10.1306/011817DIG17026

96) Riding, R., Liang, L., Braga, J.C., 2014. Millennial-scale ocean acidification and late Quaternary decline of cryptic bacterial crusts in tropical reefs. Geobiology, 12, 387–405. doi.org/10.1111/gbi.12097

97) Ridgwell, A., Schmidt, D.N., 2010. Past constraints on the vulnerability of marine calcifiers to massive carbon dioxide relase. Nat. Geo. 3, 196–200. doi:10.1038/ngeo755

98) Rigo, M., Joachimski, M.M., 2010. Palaeoecology of Late Triassic conodonts: constraints from oxygen isotopes in biogenic apatite. Acta Palaeontol. Pol. 55, 471–478. dx.doi.org/10.4202/app.2009.0100

99) Rigo, M., Preto, N., Roghi, G., Tateo, F., Mietto, P., 2007. A rise in the Carbonate Compensation Depth of western Tethys in the Carnian (Late Triassic): deep-water evidence for the Carnian Pluvial Event. Palaeogeogr. Palaeoclimatol. Palaeoecol. 246, 188–205. doi.org/10.1016/j.palaeo.2006.09.013

100) Rigo M, Mazza M, Karádi V, Nicora A., 2018. New Upper Triassic conodont biozonation of the Tethyan Realm. In: Tanner, L. H. (ed.), The Late Triassic World: Earth in a Time of Transition, Springer, Berlin.

101) Roghi, G., 2004. Palynological investigations in the Carnian of Cave del Predil area (once Raibl, Julian Alps). Rev. Palaeobot. Palynol. 132, 1–35. DOI: 10.1016/j.revpalbo.2004.03.001

102) Roghi, G., Gianolla, P., Minarelli, L., Pilati, C., Preto, N., 2010. Palynological correlation of Carnian humid pulses throughout western Tethys. Palaeogeogr. Palaeoclimatol. Palaeoecol. 290, 89–106. doi.org/10.1016/j.palaeo.2009.11.006

103) Rostási, Á., Raucsik, B., Varga, A., 2011. Palaeoenvironmental controls on the clay mineralogy of Carnian sections from the Transdanubian Range (Hungary). Palaeogeogr. Palaeoclimatol. Palaeoecol. 300, 101–112. doi.org/10.1016/j.palaeo.2010.12.013

104) Ruffell, A., Simms, M.J., Wignall, P.B., 2015. The Carnian Humid Episode of the late Triassic: a review. Geol. Mag. 153, 271–284. doi.org/10.1017/S0016756815000424

105) Russo, F., Neri, C., Mastandrea, A., Baracca, A., 1997. The mudmound nature of the Cassian platform margins of the Dolomites. A case history: the Cipit boulders from Punta

Grohmann (Sasso Piatto Massif, Northern Italy). Facies 36, 25–36. doi.org/10.1007/BF02536875

106) Rruhl, M., Kürschner, W.M., 2011. Multiple phases of carbon cycle disturbance from large igneous province formation at the Triassic–Jurassic transition. Geology 39, 431–434. doi.org/10.1130/G31680.1

107) Ruhl, M., Bonis, N.R., Reichard, G.J., Sinninghe Damsté, J.S., Kürschner, W.M., 2011. Atmospheric carbon injection linked to End-Triassic Mass Extinction. Science 333, 430–434. DOI: 10.1126/science.1204255

108) Saxby, J.D., Stephenson, L.C. 1987. Effect of an igneous intrusion on oil shale at Rundle (Australia). Chem. Geol. 63, 1–16. doi.org/10.1016/0009-2541(87)90068-4

109) Schlager, W., Schöllnberger, W., 1974. Das Prinzip stratigraphischer Wenden in der Schichtfolge der Nördlichen Kalkalpen. Mitt. Österr. Geol. Ges. 66–67, 165–193.

110) Schmidt, J.M., and Rogers, R.K., 2007, Metallogeny of the Nikolai large igneous province (LIP) in southern Alaska and its infl uence on the mineral potential of the Talkeetna Mountains, in Ridgway, K.D., et al., eds., Tectonic growth of a collisional continental margin: Crustal evolution of southern Alaska. GSA Special Paper 431, 623–648.

111) Scheuring, B.W., 1970. Palynologische und palynostratigraphische Untersuchungen des Keupers im Bölchentunnel (Solothurner Jura). Schweiz. Palaeontol. Abh. 88, 2–119.

112) Schubert, B.A., Jahren, A.H., 2012. The effect of atmospheric CO_2 concentration on carbon isotope fractionation in C3 land plants. Geochim. Cosmochim. Acta 96, 29–43. https://doi.org/10.1016/j.gca.2012.08.003

113) Simms, M.J., Ruffell, A.H., 1989. Synchroneity of climatic change and extinctions in the Late Triassic. Geology 17, 265–268. doi.org/10.1130/0091-7613(1989)017<0265:SOCCAE>2.3.CO;2

114) Simms, M.J., Ruffell, A.H., 1990. Climatic and biotic change in the Late Triassic. J. Geol. Soc. 147, 321–327. doi.org/10.1144/gsjgs.147.2.0321

115) Simms, M.J., Ruffel, A.H., Johnson, L.A., 1995. Biotic and climatic changes in the Carnian (Triassic) of Europe and adjacent areas. In: Fraser, N.C., Sues, H.-D. (Eds.), In The Shadow Of The Dinosaurs: Early Mesozoic Tetrapods. Cambridge University Press, pp. 352–365.

116) Simoneit, B.R.T., Brenner, S., Peters, K.E., Kaplan, I.R., 1978. Thermal alteration of Cretaceous black shale by basaltic intrusions in the Eastern Atlantic. Nature 273, 501–504. http://dx.doi.org/10.1038/273501a0.

117) Stampfli, G.M., Borel, G.D., 2002. A plate tectonic model for the Paleozoic and Mesozoic constrained by dynamic plate boundaries and restored synthetic oceanic isochrons. Earth Planet. Sci. Lett. 196, 17-33. doi.org/10.1016/S0012-821X(01)00588-X

118) Stefani, M., Furin, S., Gianolla, P., 2010. The changing climate framework and deposi- tional dynamics of the Triassic carbonate platforms from the Dolomites. Palaeogeogr. Palaeoclimatol. Palaeoecol. 290, 43–57. doi.org/10.1016/j.palaeo.2010.02.018

119) Stur, D., 1868. Beiträge zur Kenntniss der Geologischen Verhältnisse der Umgegend von Raibl und Kaltwasser. Jhb. K. K. Geol. Reichsanst. 18, 71–122, Wien.

120) Suess, E., 1867. Raibl. In: E. Suess, E., und Mojsisovics, E.M.v. – Studien über die Gliederung der Trias und Jurabildungen in den östichen Alpen. Jhb. K. K. Geol. Reichsanst. 17/4, 554–582, Wien.

121) Sun, Y., Wignall, P., Joachimski, M.M., Bond, D.P.G., Grasby, S.E., Lai, X.L., Wang, L.N., Zhang, Z.T., Sun, S., 2016. Climate warming, euxinia and carbon isotope perturbations during the Carnian (Triassic) Crisis in South China. Earth Planet. Sci. Lett. 444, 88–100. doi.org/10.1016/j.epsl.2016.03.037

122) Svensen, H., Planke, S., Malthe-Sørenssen, A., Jamtveit, B., Myklebust, R., Rasmussen Eidem, T., Rey, S.S., 2004. Release of methane from a vol- canic basin as mechanism for initial Eocene global warming. Nature 429, 542–545. doi:10.1038/nature02566

123) Tozer, 1967. A standard for Triassic time. Geol. Surv. Canada Bull. 156, 1–103.

124) Tozer, E.T., 1994. Canadian Triassic Ammonoid Faunas. Geol. Surv. Canada Bull. p. 467.

125) Trotter, A.J., Williams, S.I., Nicora, A., Mazza, M., Rigo, M., 2015. Long-term cycles of Triassic climate change: A new $\delta^{18}O$ record from conodont apatite. Earth Planet. Sci. Lett. 415, 165–174. doi.org/10.1016/j.epsl.2015.01.038

126) Urlichs, M., 1974, Zur Stratigraphie und Ammonitenfauna der Cassianer Schichten von Cassian (Dolomiten/Italien). Schrift. Erdwiss. Komm. Österr. Ak. Wiss., 2, 207–222.

127) Urlichs, M., 1994. Trachyceras Laube 1869 (Ammonoidea) aus dem Unterkarn (Obertrias) der Dolomiten (Italien). Stuttg. Beitr. Naturk., ser. B (Geol. Paläont.) 217, 1–55.

128) Urlichs, M., 2017. Revision of some stratigraphically relevant ammonoids from the Cassian Formation (Latest Ladinian-Early Carnian, Triassic) of St. Cassian (Dolomites. Italy). N. Jb. Geol. Paläont. Abh. 283/2, 173–204. doi.org/10.1127/njgpa/2017/0635

129) van de Schootbrugge, B., Payne, J.L., Tomasovych, A., Pross, J., Fiebig, J., Benbrahim, M., Föllmi, K.B., Quan, T.M., 2008. Carbon cycle perturbation and stabilization in the wake of the Triassic–Jurassic boundary mass-extinction event. Geochem. Geophys. Geosyst. 9 (4), Q04028. doi.org/10.1029/2007GC001914

130) Van der Eem, J.G.L.A., 1983. Aspects of Middle and Late Triassic Palynology. 6. Palynological investigations in the Ladinian and Lower Karnian of the WesternDolomites, Italy. Rev. Palaeobot. Palynol. 39, 189–300. doi.org/10.1016/0034-6667(83)90016-7

131) Vörös, A. 1998: A Balaton-felvidék triász ammonoideái és biosztratigráfiája. Studia Nat. 12, 105.

132) Wignall, P.B., 2001. Large igneous provinces and mass extinctions. Earth-Sci. Rev. 53, 1–33. doi.org/10.1016/S0012-8252(00)00037-4

133) Xu, G., Hannah, J.L., Stein, H.J.,Mørkd, A., Os Vigran, J., Bingen, B., Schutte, D., Lundschieng, B.A., 2014. Cause of Upper Triassic climate crisis revealed by Re–Os geochemistry of Boreal black shales. Palaeogeogr. Palaeoclimatol. Palaeoecol. 395, 222–232. doi.org/10.1016/j.palaeo.2013.12.027

134) Zachos, J.C., Rohl, U., Schellenberg, S.A., Sluijs, A., Hodell, D.A., Kelly, D.C., Thomas, E., Nicolo, M., Raffi, I., Lourens, L.J., McCarren, H., Kroon, D., 2005. Rapid ocean acidification of the ocean during the Paleocene-Eocene thermal maximum. Science 308, 1611–1615. DOI: 10.1126/science.1109004

135) Zeebe, R.E., Zachos, J.C., Dickens, G.R., 2009. Carbon dioxide forcing alone insufficient to explain Palaeocene–Eocene Thermal Maximum warming. Nat. Geo. 2, 576–580. doi:10.1038/ngeo578

136) Zhang, Y., Li, M., Ogg, J., Montgomery, P., Huang, C., Chen, Z.-Q., Shi, Z., Enos, P., Lehrmann, D.J., 2015. Cycle-calibrated Magnetostratigraphy of middle Carnian from South China: Implications for Late Triassic Time Scale and Termination of the Yangtze Platform. Palaeogeogr. Palaeoclimatol. Palaeoecol. 436, 135–166. doi.org/10.1016/j.palaeo.2015.05.033